Copyright Warning & Restrictions

The copyright law of the United States (Title 17, United States Code) governs the making of photocopies or other reproductions of copyrighted material.

Under certain conditions specified in the law, libraries and archives are authorized to furnish a photocopy or other reproduction. One of these specified conditions is that the photocopy or reproduction is not to be "used for any purpose other than private study, scholarship, or research." If a, user makes a request for, or later uses, a photocopy or reproduction for purposes in excess of "fair use" that user may be liable for copyright infringement,

This institution reserves the right to refuse to accept a copying order if, in its judgment, fulfillment of the order would involve violation of copyright law.

Please Note: The author retains the copyright while the New Jersey Institute of Technology reserves the right to distribute this thesis or dissertation

Printing note: If you do not wish to print this page, then select "Pages from: first page # to: last page #" on the print dialog screen

NJIT New Jersey's Science & Technology University

The Van Houten library has removed some of the personal information and all signatures from the approval page and biographical sketches of theses and dissertations in order to protect the identity of NJIT graduates and faculty.

ABSTRACT

IMAGE MORPHOLOGICAL PROCESSING

by
Vijayalakshmi Gaddipati

Mathematical Morphology with applications in image processing and analysis has been becoming increasingly important in today's technology. Mathematical Morphological operations, which are based on set theory, can extract object features by suitably shaped structuring elements. Mathematical Morphological filters are combinations of morphological operations that transform an image into a quantitative description of its geometrical structure based on structuring elements. Important applications of morphological operations are shape description, shape recognition, nonlinear filtering, industrial parts inspection, and medical image processing.

In this dissertation, basic morphological operations, properties and fuzzy morphology are reviewed. Existing techniques for solving corner and edge detection are presented. A new approach to solve corner detection using regulated mathematical morphology is presented and is shown that it is more efficient in binary images than the existing mathematical morphology based asymmetric closing for corner detection.

A new class of morphological operations called sweep mathematical morphological operations is developed. The theoretical framework for representation, computation and analysis of sweep morphology is presented. The basic sweep morphological operations, sweep dilation and sweep erosion, are defined and their properties are studied. It is shown that considering only the boundaries and performing

operations on the boundaries can substantially reduce the computation. Various applications of this new class of morphological operations are discussed, including the blending of swept surfaces with deformations, image enhancement, edge linking and shortest path planning for rotating objects.

Sweep mathematical morphology is an efficient tool for geometric modeling and representation. The sweep dilation/erosion provides a natural representation of sweep motion in the manufacturing processes. A set of grammatical rules that govern the generation of objects belonging to the same group are defined. Earley's parser serves in the screening process to determine whether a pattern is a part of the language. Finally, summary and future research of this dissertation are provided.

IMAGE MORPHOLOGICAL PROCESSING

by
Vijayalakshmi Gaddipati

A Dissertation
Submitted to the Faculty of
New Jersey Institute of Technology
in Partial Fulfillment of the Requirements for the Degree of
Doctor of Philosophy in Computer Science

Department of Computer Science

May 2003

Copyright © 2003 by Vijayalakshmi Gaddipati

ALL RIGHTS RESERVED

APPROVAL PAGE

IMAGE MORPHOLOGICAL PROCESSING

Vijayalakshmi Gaddipati

Dr. Frank Shih, Dissertation Advisor — Date
Professor of Computer Science, Associate Chairman of Computer Science Department, NJIT

Dr. James A.M. McHugh, Committee Member — Date
Professor of Computer Science, Acting Chairman of Computer Science Department, NJIT

Dr. Yun-qing Shi, Committee Member — Date
Professor of Electrical and Computer Engineering, NJIT

Dr. Chengjun Liu, Committee Member — Date
Assistant Professor of Computer Science, NJIT

Dr. Sven Loncaric, Committee Member — Date
Assistant Professor of Electrical and Computer Engineering, NJIT

BIOGRAPHICAL SKETCH

Author: Vijayalakshmi Gaddipati

Degree: Doctor of Philosophy

Date: May 2003

Undergraduate and Graduate Education:

- Doctor of Philosophy in Computer Science
  New Jersey Institute of Technology, Newark, NJ, 2003

- Master of Technology in Computer Science
  University of Hyderabad, Hyderabad, India, 1988

- Master of Science in Mathematics
  University of Hyderabad, Hyderabad, India, 1985

Major: Computer Science

Presentations and Publications:

F. Y. Shih, V. Gaddipati and D. Blackmore, "Error analysis of surface fitting for swept volumes," *Proc. Japan-USA* Symp. Flexible Automation, pp. 733-737, Kobe, Japan, July 1994.

Frank Y. Shih and Vijayalakshmi Gaddipati, "General sweep mathematical morphology," *Pattern Recognition,* vol. 36, no. 7, pp. 1489-1500, July 2003.

Frank Y. Shih and Vijayalakshmi Gaddipati, "Geometric modeling and representation based on sweep mathematical morphology," *submitted to Information Systems,* 2003.

This dissertation is dedicated to
my parents, my husband and my children,
Sumedha and Raviteja.

ACKNOWLEDGMENTS

The author would like to express her sincere appreciation to her research advisor Dr. Frank Y. Shih, for his advice and guidance during the years of doctoral research. His valuable time and insight were instrumental to the author in this research.

Special thanks to Dr. James McHugh, Dr. Yun-qing Shi, Dr. Chengjun Liu, and Dr. Sven Loncaric for actively participating as members of the committee and providing valuable advice.

The author would like to thank the CIS department for the financial support during the period of research and appreciates the help and suggestions received from Dr. Fadi Deek during the teaching assistant years. The author would like to thank Agere Systems for the financial support through tuition assistance plan and especially to her technical manager Mr. Martin Trew for his support. The author extends special thanks to her fellow students for their assistance and support, in particular to Artur Kowalski, Aruna Kolla, Yugyung Lee, Maria Cecilia Flores, Bo-Chao Chen, Christopher Pu, Jenlong Moh and Shushyan Chen.

Special thanks to the author's family members for their never ending support, understanding, and encouragement during the years of advance studies. The author is grateful to her beloved husband Sitaramaiah Kanthamneni for his love and consistent support.

TABLE OF CONTENTS

Chapter		Page
1	INTRODUCTION	1
	1.1 Binary Morphological Operations	3
	1.2 Gray Scale Morphological Operations	9
	1.3 Fuzzy Mathematical Morphology	11
2	CORNER DETECTION	17
	2.1 Introduction	17
	2.2 Related Research	18
	2.3 Asymmetrical Closing for Corner Detection	19
	2.4 Regulated Morphological Operations	23
	2.4.1 Regulated Morphological Operators for Corner Detection	25
	2.5 Conclusions	28
3	GENERAL SWEEP MATHEMATICAL MORPHOLOGY	30
	3.1 Introduction	30
	3.2 Theoretical Development of General Sweep Mathematical Morphology	32
	3.2.1 The Computation of Traditional Morphology	33
	3.2.2 The General Sweep Mathematical Morphology	35
	3.2.3 The Properties of Sweep Morphological Operations	39
	3.3 Blending of Swept Surfaces with Deformations	42
	3.4 Image Enhancement	45
	3.5 Edge Linking	48
	3.5.1 Edge Linking using Sweep Morphology	50
	3.6 Shortest Path Planning for Mobile Robot	58
	3.7 Conclusions	60

TABLE OF CONTENTS
(Continued)

Chapter			Page
4	GEOMETRIC MODELING AND REPRESENTATION		61
	4.1	Introduction	61
	4.2	Geometric Modeling and Sweep Mathematical Morphology	63
		4.2.1 Tolerancing Expression	63
		4.2.2 Sweep Surface Modeling	65
	4.3	Formal Languages and Sweep Mathematical Morphology	66
	4.4	Representation Scheme	67
		4.4.1 Two-dimensional Attributes	67
		4.4.2 Three-dimensional Attributes	69
	4.5	Grammars	74
		4.5.1 Two-dimensional Attributes	74
		4.5.2 Three-dimensional Attributes	75
	4.6	Parsing Algorithm	78
	4.7	Conclusions	81
5	SUMMARY AND FUTURE RESEARCH		82
REFERENCES			85

LIST OF FIGURES

Figure		Page
1.1	Example of dilation of set A by structuring element B.	4
1.2	Example of erosion of set A by structuring element B.	5
1.3	Example of opening of set A by structuring element B.	7
1.4	Example of closing of set A by structuring element B.	7
1.5	(a) Original binary image (b) Structuring element (c) Result of dilation (d) Result of erosion (e) Result of closing (f) Result of opening.	8
1.6	(a) Original image (b) Structuring element (c) Result of dilation (d) Result of erosion (e) Result of closing (f) Result of opening.	10
2.1	Opening and closing: (a) test pattern (b) erosion (c) opening (d) dilation (e) closing (f) asymmetrical closing.	20
2.2	(a) Structuring element + (b) structuring element $\diamond$ (c) structuring element $\times$ (d) structuring element $\square$.	21
2.3	(a) Triangle binary image (b) Corners with Laganiere's operator (c) Corners with modified Laganiere's operator.	22
2.4	(a) Grayscale image (b) Corners with Laganiere's operator (c) Corners with modified Laganiere's operator.	22
2.5	(a) Original shape (b) Structuring element (c) Ordinary dilation (d) Regulated dilation with a strictness of 2.	24
2.6	(a) Original shape (b) Structuring element (c) Ordinary erosion (d) Regulated erosion with a strictness of 2.	25
2.7	5×5 structuring element.	25
2.8	(a) Circle (b) Corners with regulated closing with strictness 2.	26
2.9	(a) Square (b) Corners with regulated closing with strictness 2.	26
2.10	(a) Triangle (b) Corners with regulated closing with strictness 2.	27
2.11	(a) Image (b) Corners with regulated closing with strictness 2.	27

LIST OF FIGURES
(Continued)

Figure		Page
2.12	(a) Tree image (b)) Corners with regulated closing with strictness 2 (c) Corners with regulated closing with strictness 3.	28
3.1	(a) An open curve path, (b) a structuring element, (c) result of a traditional morphological dilation, (d) result of a sweep morphological dilation.	36
3.2	(a) Traditional erosion (b) sweep erosion.	38
3.3	Sweeping of a square along a trajectory with deformation to a circle.	444
3.4	Structuring element assignment using general sweep morphology.	46
3.5	The elliptic structuring element.	50
3.6	(a) Input signal (b) Sweep dilation with elliptical structuring elements.	51
3.7	(a) Original elliptical edge and (b) Its randomly discontinuous edge	53
3.8	Using circular structuring elements in 5 iterations with (a) r=3, (b) r=5, and (c) r=10.	54
3.9	Using the sweep morphological edge-linking algorithm.	55
3.10	(a) The edge of an industrial part, (b) Its randomly discontinuous edge, and (c) Using the sweep morphological edge-linking algorithm	56
3.11	(a) Part edge with added uniform noise, (b) Part edge after removing noise, and (c) Using the sweep morphological edge-linking algorithm.	57
3.12	(a) Face image with the originally detected broken edge and (b) Face image with the edge linked by the sweep morphological edge-linking algorithm.	58
3.13	Shortest path of an H-shaped car by using the sweep (rotational) morphology.	59
4.1	Tolerance zones. (a) An annular tolerance zone that corresponds to a circular hole. (b) A tolerance zone for an elongated slot.	64
4.2	An example of adding tolerance by a morphological dilation.	65
4.3	Modeling of sweep surface.	66
4.4	The Decomposition of two-dimensional attributes.	68

LIST OF FIGURES
(Continued)

Figure		Page
4.5	The Decomposition of three-dimensional attributes.	69
4.6	Sweep dilation of a rectangle with a corner truncated by a circle.	70
4.7	Sweeping of a square along a trajectory with deformation to a circle.	71
4.8	Sweep dilation of a rectangle with a circular hole.	72
4.9	Machining with a round bottom tool.	73
4.10	An example of swept surface.	81

CHAPTER 1

INTRODUCTION

Mathematical Morphology provides an approach to the processing of digital images based on shape. Mathematical Morphology is a topological and geometrical based approach for image analysis. It provides powerful tools for extracting geometrical structures and representing shapes in many applications.

Mathematical morphology is becoming increasingly important in image processing and computer vision applications for the identification and decomposition of objects, object features, and object surface defects. Morphological operators can simplify image data, preserving their essential shape characteristics, and can eliminate irrelevancies. Mathematical Morphology is a set-theoretical method that was first introduced by Matheron [39] and Serra [63] at Paris School of Mines, France around 1964.

Mathematical Morphological operations can be employed for corner and edge detection, segmentation, and enhancement of images, which provides for the systematic alteration of the geometric content of an image while maintaining the stability of important geometric characteristics. Moreover, there exists a well-defined morphological algebra that can be employed for representation and optimization and it is possible to express digital algorithms in terms of a very small class of primitive morphological operations.

Maragos and Ziff [36] showed that many composite morphological systems, such as morphological edge detection, peak/valley extraction, skeletonization, and shape-size distributions obey linear superposition, which is called *threshold-linear superposition.*

Namely, the output is the sum of outputs due to input binary images that result from thresholding the input gray-level images at all levels. The threshold decomposition architecture and stacking property are introduced by Shih and Mitchell [68], which allows the implementation of the architecture that gray-scale operations can be decomposed into binary operation with the same dimensionality as the original operations. Shih and Mitchell [69][70] presented techniques for decomposing big gray-scale morphological structuring elements into combined structures of segmented small components. The decomposition is suitable for parallel-pipelined architecture and the technique will allow us to design any kind and size of gray-scale structuring elements.

Edge operators based on gray-scale morphological operations are introduced by Lee, Haralick and Shapiro [31]. The simplest morphological edge detectors are the dilation residue and erosion residue operators. Different combinations of these two operators is also introduced and justified. The blur-minimum morphological edge detector is defined whose inherent noise sensitivity is less than the dilation and erosion residue operators. The alternating sequential filter edge detector proposed by Song and Neuvo [79] overcomes the problem of localizing the edges correctly introduced by the blur-minimum morphological edge detector. Not all edges with various fineness regarding spectral contrast and spatial geometry can be detected by single operator and Chanda and *et al.* [5] have proposed a multi-scale morphological edge detector that can differentiate the fine variations of gray-level surface, and yet can remove noise.

Shape decomposition is a very important issue in image processing and pattern recognition. Shape decomposition is to decompose binary objects into a union of *simple* objects. The decomposition should be unique, translation, scaling, and rotation invariant.

Some morphological approach [48][49] is to use the structuring elements as the simplest object component and to analyze an image as a union of the structuring elements. This approach is based on the structuring elements used, therefore, an object is represented by those structuring elements.

Shape description describes the object according to its shape geometric features. The shape of an object refers to its profile and physical structure. These characteristics can be represented by the boundary, region, moment, and structural representations. These representations can be used for matching shapes, recognizing objects, or making measurements on the shape characteristics. Therefore, the shape description is a very active and important issue in image processing, computer vision, and pattern recognition during recent decades.

In this chapter, the basic morphological operations of dilation and erosion in an N-dimensional Euclidean space and their derived operations of opening and closing and their properties are reviewed. Later various techniques that have been developed in mathematical morphology are discussed.

1.1 Binary Morphological Operations

The language of mathematical morphology is set theory. Given two sets A, $B \subset Z^{N,}$ the morphological dilation of a set A by a set of structuring element B is defined [21] by

$$A \oplus B = \{a + b \mid a \in A, b \in B\} = \cup_{b \in B} A_{b,} \tag{1.1}$$

where A_b is the translation of a set A by a vector b: $A_b = \{x \mid x = a+b, a \in A, x \in Z^N\}$. The dilation operation can be interpreted as the union of all the possible shifts for which the reflected and shifted B intersects A. That is,

$$A \oplus B = \{x \mid (A \cap (\hat{B})_x \neq 0) \tag{1.2}$$

where $\hat{B}$ is the reflection of B given by $\hat{B} = \{x \mid \exists\, b \in B: x = -b\}$.

An example of dilation is given in Figure 1.1.

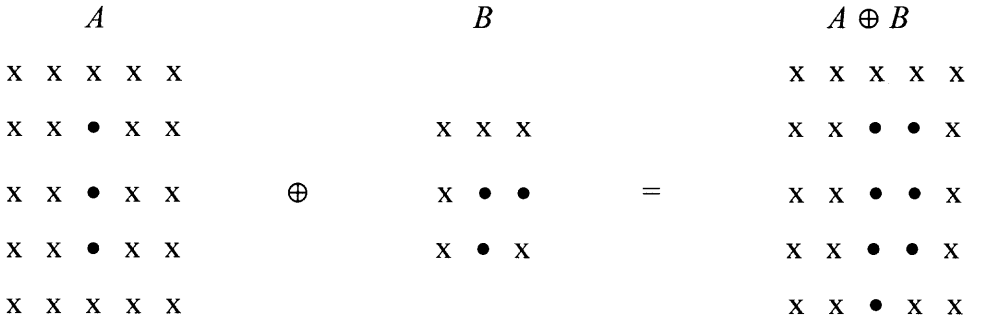

Figure 1.1 Example of dilation of set A by structuring element B.

Given two sets A, $B \subset Z^N$, the morphological erosion of a set A by a set of structuring element B is defined [21] by

$$A \ominus B = \{x \mid \forall\, b \in B\, \exists\, a \in A: x = a - b\} = \cap_{b \in B} (A)_{-b} \tag{1.3}$$

The erosion of A by B results in an erosion of the shapes in A. The erosion operation can be interpreted as the union of all the possible shifts for which the shifted B is contained completely within A. That is,

$$A \ominus B = \{x \mid (A^c \cap (B)_x = 0) \tag{1.4}$$

where A^c is the complement of A defined by $A^c = \{x \mid x \notin A\}$.

An example of erosion is given in Figure 1.2.

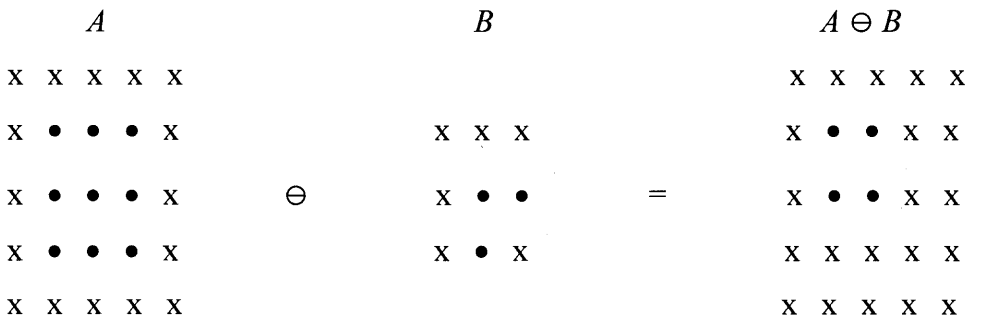

Figure 1.2 Example of erosion of set A by structuring element B.

Dilation and erosion posses several properties, which are given below. For proofs of these the reader may refer the references [11][21][63][64].

(1) The dilation and erosion are dual operations:

$$A \oplus B = (A^c \ominus \hat{B})^c$$

$$A \ominus B = (A^c \oplus \hat{B})^c \tag{1.5}$$

(2) Commutative property:

$$A \oplus B = B \oplus A \tag{1.6}$$

(3) Associative property:

$$A \oplus (B \oplus C) = (A \oplus B) \oplus C \tag{1.7}$$

(4) Translation invariance:

$$A_z \oplus B = (A \oplus B)_z \tag{1.8}$$

$$A \oplus B_z = (A \oplus B)_z \tag{1.9}$$

$$A_z \ominus B = (A \ominus B)_z \tag{1.10}$$

$$A \ominus B_z = (A \ominus B)_{-z} \tag{1.11}$$

(5) Increasing property:

$$A \subseteq B \Rightarrow A \oplus C \subseteq B \oplus C \tag{1.12}$$

$$A \subseteq B \Rightarrow A \ominus C \subseteq B \ominus C \tag{1.13}$$

(6) Distributive property:

$$(A \cup B) \oplus C = (A \oplus C) \cup (B \oplus C) \tag{1.14}$$

$$A \oplus (B \cup C) = (A \oplus B) \cup (A \oplus C) \tag{1.15}$$

$$A \ominus (B \cup C) = (A \ominus B) \cap (A \ominus C) \tag{1.16}$$

$$(B \cap C) \ominus A = (B \ominus A) \cap (C \ominus A) \tag{1.17}$$

The derived morphological operations opening and closing are defined as follows. Given two sets A, $B \subset Z^N$, the morphological *opening* of a set A by a set of structuring element B is defined [21] by

$$A \circ B = (A \ominus B) \oplus B \tag{1.18}$$

and the morphological *closing* of a set A by a set of structuring element B is defined [21] by

$$A \bullet B = (A \oplus B) \ominus B \tag{1.19}$$

Examples of opening and closing are given as follows.

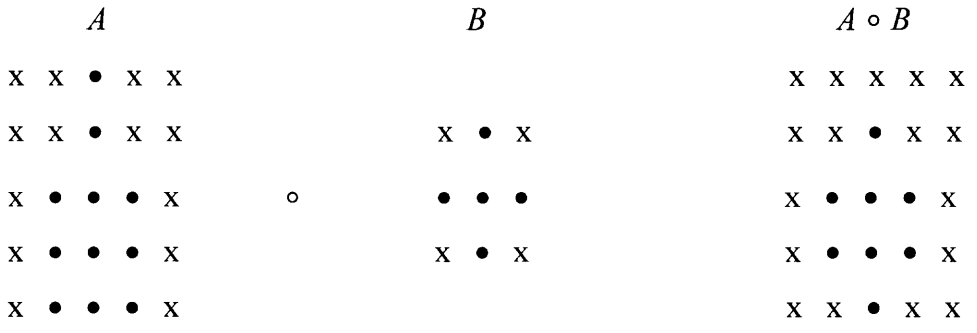

Figure 1.3 Example of opening of set *A* by structuring element *B*.

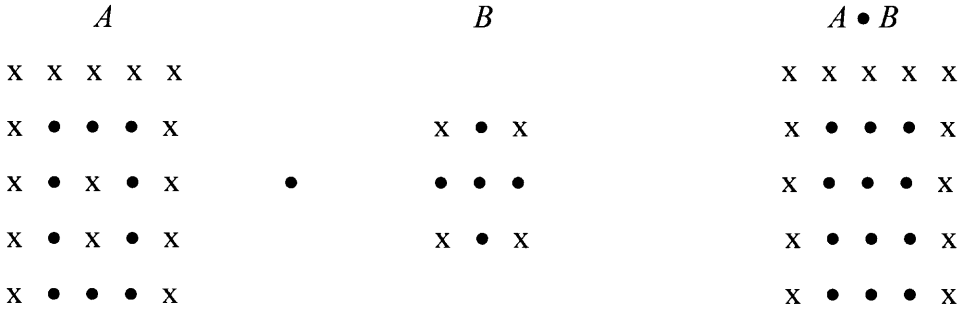

Figure 1.4 Example of closing of set *A* by structuring element *B*.

Figure 1.5 illustrates dilation, erosion, closing and opening operations by a 3×3 structuring element on a binary image of character "**B**".

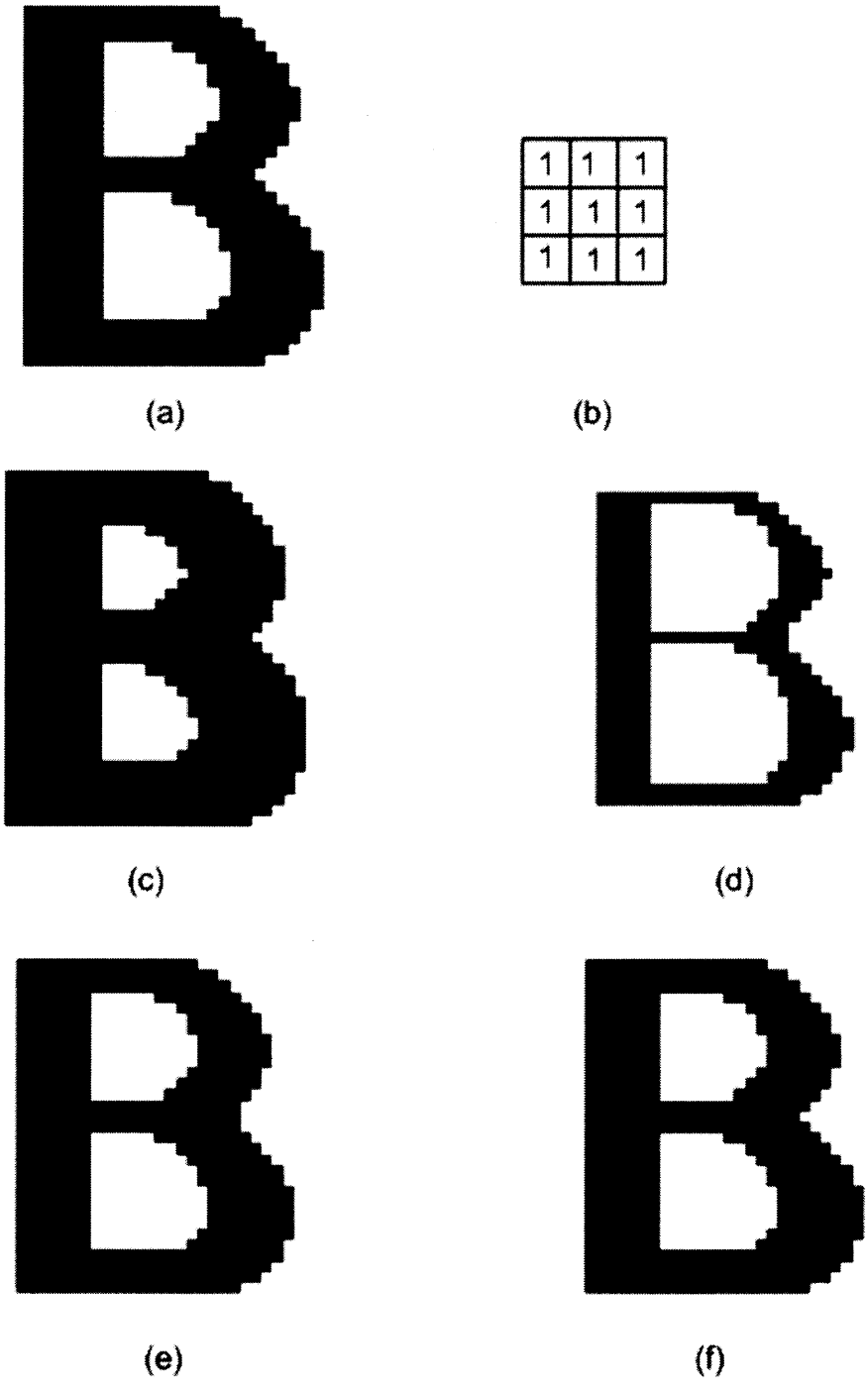

Figure 1.5 (a) Original binary image (b) Structuring element (c) Result of dilation (d) Result of erosion (e) Result of closing (f) Result of opening.

1.2 Gray Scale Morphological Operations

The notions and morphological transformations of a binary image can also be extended to gray-scale images. Let f and k be the gray-scale image and the structuring elements. The gray-scale morphological dilation, erosion, opening and closing are defined as follows, where $x - z \in f$ and $z \in k$.

$$(f \oplus k)(x) = \max \{ f(x\text{-}z) + k(z)\} \tag{1.20}$$

$$(f \ominus k)(x) = \min \{f(x+z) - k(z)\} \tag{1.21}$$

$$f \circ k = (f \ominus k) \oplus k \tag{1.22}$$

$$f \bullet k = (f \oplus k) \ominus k \tag{1.23}$$

Interested readers may refer [11][21][63][64] for more in detail gray-scale morphology and its properties. Figure 1.6 illustrates dilation, erosion, closing and opening operations by a 3×3 structuring element on a gray-level image.

(a)

1	1	1
1	1	1
1	1	1

(b)

(c)

(d)

(e)

(f)

Figure 1.6 (a) Original image (b) Structuring element (c) Result of dilation (d) Result of erosion (e) Result of closing (f) Result of opening.

1.3 Fuzzy Mathematical Morphology

Fuzzy set theory has found a promising field of application in the domain of digital image processing, since fuzziness is an intrinsic property of images. In this images are modeled as fuzzy subsets of the Euclidean plane or Cartesian grid, and the morphological operators are defined in terms of a fuzzy index function. Fuzzy sets were introduced by Zadeh [85] and elementary operations, intersection, union, complementation, inclusion, etc., were defined. The fuzzy set theoretic operations are defined as follows. The characteristic function of a crisp set A, denoted as μ_A: $U \rightarrow \{0,1\}$, is defined to be

$$\mu_A(x) = \begin{cases} 1 & \text{if } x \in A \\ 0 & \text{otherwise} \end{cases} \tag{1.24}$$

The membership function of a fuzzy set A, denoted by μ_A: $U \rightarrow [0,1]$, is defined in such a way that $\mu_A(x)$ denotes the degree to which x belongs to A. The higher the value of $\mu_A(x)$, the more x belongs to A; and conversely, the smaller the value of $\mu_A(x)$, the less likelihood of x being in the set A. For further details see Zadeh [85][86].

The union, intersection, difference, and complement operations on crisp as well as fuzzy sets can be defined in terms of their characteristic/membership functions:

$$\mu_{A \cup B}(x) = \max[\mu_A(x), \mu_B(x)] \tag{1.25}$$

$$\mu_{A \cap B}(x) = \min[\mu_A(x), \mu_B(x)] \tag{1.26}$$

$$\mu_{A \setminus B}(x) = \min[\mu_A(x), 1 - \mu_B(x)] \tag{1.27}$$

$$\mu_A^c(x) = 1 - \mu_A(x) \tag{1.28}$$

The subset relation can be rephrased as

$$A \subseteq B \Leftrightarrow \mu_B = \max[\mu_A, \mu_B] \Leftrightarrow \mu_A = \min[\mu_A, \mu_B] \tag{1.29}$$

The *support* of a set A, denoted as $\mathcal{S}(A)$, is a crisp set of those elements of U which belong to A with some certainty:

$$\mathcal{S}(A) = \{x : \mu_A(x) > 0\} \tag{1.30}$$

The *translation* of a set A by a vector $v \in U$, denoted by $\mathcal{T}(A; v)$, is defined as

$$\mu_{\mathcal{T}(A;v)}(x) = \mu_A(x - v) \tag{1.31}$$

The *reflection* of set A, denoted by $\hat{A}$, defined as

$$\mu_{\hat{A}}(x) = \mu_A(-x) \tag{1.32}$$

The *scalar addition* of a fuzzy set A and a constant α, denoted as $A \Diamond \alpha$, is defined as

$$\mu_{A\Diamond\alpha}(x) = \min(1, \max[0, \mu_A(x) + \alpha]) \tag{1.33}$$

Giles [19] proposed fuzzy operations, *bold union*, $X \Delta Y$ of two sets X and Y as

$$\mu_{X\Delta Y}(z) = \min[1, \mu_X(z), \mu_Y(z)] \tag{1.34}$$

and *bold intersection* $X \nabla Y$ as

$$\mu_{X\nabla Y}(z) = \max[0, \mu_X(z), \mu_Y(z) - 1] \tag{1.35}$$

If X and Y are crisp sets, then $X \Delta Y \equiv X \cup Y$ and $X \nabla Y \equiv X \cap Y$.

An *index function* I: $2^U \times 2^U \rightarrow \{0, 1\}$ is defined as

$$I(A, B) = \begin{cases} 1 & \text{if } A \subseteq B \\ 0 & \text{otherwise} \end{cases} \tag{1.36}$$

The above equation can be rewritten so as to express the index function directly in terms of characteristic functions:

$$\begin{aligned} I(A, B) &= \inf_{x \in A} \mu_B(x) \\ &= \min [\inf_{x \in A} \mu_B(x), \inf_{x \notin A} 1] \\ &= \inf_{x \in U} \mu_{A^c \Delta B}(x) \end{aligned} \tag{1.37}$$

The last relation follows because for crisp sets the bold union has the following properties:

$x \in A \Rightarrow \mu_{A^c \Delta B}(x) = \mu_B(x)$

$x \notin A \Rightarrow \mu_{A^c \Delta B}(x) = 1.$

The index function can be generalized, so that $I(A, B)$ gives the degree to which A is a subset of B. The formulation given in the equation (1.37) suffices for this purpose. The properties of morphological operations will be induced by the properties of the index function.

Consider any two fuzzy subsets $A, B \subset U$; index function $I(A, B)$ for different values of set B, and set A essentially fixed and $A \neq \varnothing$. The properties (axioms) for index the function to satisfy are as follows:

$I(A, B) \in [0, 1]$.

If A and B are crisp sets, then $I(A, B) \in \{0, 1\}$.

$A \subseteq B \Leftrightarrow I(A, B) = 1.$

If $B \subseteq C$, then $I(A, B) \leq I(A, C)$.

If $B \subseteq C$, then $I(C, A) \leq I(B, A)$.

$A \subseteq B \Leftrightarrow \mathfrak{I}(A; v) \subseteq \mathfrak{I}(B; v)$; i.e., $I(A, B) = I(\mathfrak{I}(A; v), \mathfrak{I}(B; v))$ – preserve the translation-invariant nature of subset relation.

$A \subseteq B \Leftrightarrow A^c \subseteq B^c$; i.e., $I(A, B) = I(A^c, B^c)$ – preserve the identity.

$I(A, B) = I(\hat{A}, \hat{B})$ - invariant under reflection.

If B and C are subsets of A, then so is $B \cup C$. The converse also holds:

$(B \subseteq A) \wedge (C \subseteq A) \Leftrightarrow (B \cup C) \subseteq A$; i.e., $I(B \cup C, A) = \min[I(B, A), I(C, A)]$.

Similarly, $(A \subseteq B) \wedge (A \subseteq C) \Leftrightarrow A \subseteq (B \cap C)$; i.e., $I(A, B \cap C) = \min[I(A, B), I(A, C)]$.

The fuzzy morphological operations erosion, dilation, opening and closing are defined in terms of index function as follows [77]. The *erosion* of a set A by another set B, denoted as $A \ominus B$ is defined by

$\mu_{A \ominus B}(x) = I(\mathfrak{I}(B; x), A)$.

The *dilation* of a set A by another set B, denoted as $A \oplus B$ is defined by

$$\mu_{A \oplus B}(x) = \mu_{(A^c \ominus \hat{B})^c}(x)$$

$$= 1 - \mu_{(A^c \ominus \hat{B})}(x)$$

$$= I^c(\mathfrak{I}(\hat{B}; x), A^c).$$

$$= \sup_{z \in U} \max[0, \mu_{\mathfrak{I}(\hat{B}; x)}(z) + \mu_A(z) - 1]$$

The *opening* of a set A by another set B, denoted as $A \circ B$ is defined by

$A \circ B = (A \ominus B) \oplus B$.

And the *closing* of a set A by another set B, denoted as $A \bullet B$ is defined by

$A \bullet B = (A \oplus B) \ominus B$.

The fuzzy morphological operations are illustrated in following examples. The area of interest in a given image is represented by a rectangle and the membership values within this rectangular region are specified in a matrix format. The membership values outside this region are assumed to be fixed and this value is specified as a superscript of the matrix and the coordinates of the topmost-leftmost element of the matrix as subscript.

Example 1:

$$A = \begin{bmatrix} 0.2 & 1.0 & 0.8 & 0.1 \\ 0.3 & 0.9 & 0.9 & 0.2 \\ 0.1 & 0.9 & 1.0 & 0.3 \end{bmatrix}^{0.0}_{(0,0)} \quad \text{and} \quad B = \begin{bmatrix} 0.8 & 0.9 \end{bmatrix}^{0.0}_{(0,0)}$$

Since the structuring element fits entirely under the image when it translated by (1, -1), $A \ominus B(1, -1) = 1.0$. Similarly, $A \ominus B(1, -2) = 1.0$. For vector (1, 0), even though $\mathfrak{I}(B;1,0) \not\subseteq A$, the subset relationship almost holds:

$$A \cap \mathfrak{I}(B; 1, 0) = (0.8 \;\; 0.8)_{(1,0)} \approx \mathfrak{I}(B; 1, 0).$$

Therefore, a relatively high value of $A \ominus B(1, 0)$ is expected.

$$I[\mathfrak{I}(B; 1, 0), A] = \min \{\min [1, 1 + 0.2], \min[1, 0.8 + 0.1]\} = 0.9.$$

Thus, $A \ominus B(1, 0) = 0.9$. Proceeding along this line, the eroded image is obtained as

$$A \ominus B = \begin{bmatrix} 0.2 & 0.4 & 0.9 & 0.2 \\ 0.2 & 0.5 & 1.0 & 0.3 \\ 0.2 & 0.3 & 1.0 & 0.4 \end{bmatrix}^{0.1}_{(-1,0)}$$

And by appropriate thresholding the image is obtained as

$$A \ominus B = \begin{bmatrix} 0.9 \\ 1.0 \\ 1.0 \end{bmatrix}^{0.0}_{(1,0)}$$

Example 2:

$$A = \begin{bmatrix} 0.7 \\ 0.9 \\ 0.8 \end{bmatrix}^{0.0}_{(0,0)} \quad \text{and} \quad B = \begin{bmatrix} 0.8 & 0.9 \end{bmatrix}^{0.0}_{(0,0)}$$

$$I^c(\Im(\hat{B};x),A^c)=\begin{cases}0.5 & \text{if } x=(0,0)\\ 0.6 & \text{if } x=(1,0),(0,-2)\\ 0.7 & \text{if } x=(0,-1),(1,-2)\\ 0.8 & \text{if } x=(1,-1)\\ 0.0 & \text{otherwise}\end{cases}$$

Hence,

$$A\oplus B=\begin{bmatrix}0.5 & 0.6\\ 0.7 & 0.8\\ 0.6 & 0.7\end{bmatrix}^{0.0}_{(0,0)}$$

Example 3:

Consider the image from Example 1.

$$P\equiv A\ominus B=\begin{bmatrix}0.2 & 0.4 & 0.9 & 0.2\\ 0.2 & 0.5 & 1.0 & 0.3\\ 0.2 & 0.3 & 1.0 & 0.4\end{bmatrix}^{0.1}_{(-1,0)}$$

Therefore,

$$P^c\ominus\hat{B}=\begin{bmatrix}0.8 & 0.3 & 0.2 & 0.9\\ 0.7 & 0.2 & 0.1 & 0.8\\ 0.9 & 0.2 & 0.1 & 0.7\end{bmatrix}^{1.0}_{(0,0)}$$

Hence,

$$\mathrm{A}\circ B=(P^c\ominus\hat{B})^c=\begin{bmatrix}0.2 & 0.7 & 0.8 & 0.1\\ 0.3 & 0.8 & 0.9 & 0.2\\ 0.1 & 0.8 & 0.9 & 0.3\end{bmatrix}^{0.0}_{(-1,0)}$$

Upon appropriate thresholding, image is obtained as

$$\mathrm{A}\circ B=\begin{bmatrix}0.7 & 0.8\\ 0.8 & 0.9\\ 0.8 & 0.9\end{bmatrix}^{0.0}_{(-1,0)}$$

CHAPTER 2

CORNER DETECTION

2.1 Introduction

The corners of an object are frequently employed in the recognition of objects by computer [13][45][50][58]. Given a digital image of an object, a typical approach to detecting its corners involves first segmenting the object (by thresholding or some similar method), extracting its boundary as a chain code, and then searching for significant turnings in the boundary. Rutkowski and Rosenfeld [51], and references cited therein, provide a good survey of such techniques. However, most approaches work directly at the grayscale level [2][10][12][22][23][26][42][44][51][57][78][88].

These methods usually use local measurements in order to obtain corner strength. Non-maxima suppression and thresholding lead then to a binary map showing where corners have been detected. An accuracy of few pixels and a relatively high level of false positives usually characterize these corner finders.

One of the difficulties with corner detection lies in the corner definition itself. A restrictive description simply defines corner as the junction of two homogeneous regions separated by a high-curvature boundary. This definition is incomplete since it does not include X, Y and T-junctions that should also be categorized as corners since they might be the image of 3D corners (intersection of planes in space). A less right definition assimilates corners to points with high derivatives in several directions. This is a very loose description of the term corner since several "non-corner" points fall into this category.

This chapter proposes a corner detector based on regulated mathematical morphology. The next section is a review of existing corner detectors. Section 3 describes the asymmetrical closing proposed by Laganiere and its shortcomings. Section 4 describes the regulated morphological operators as defined by Agam and Dinstein and how these regulated dilation and erosion can be used for corner detection. Conclusions are made in Section 5.

2.2 Related Research

Corner detection techniques can be classified into two major categories: boundary-based approaches and gray-level approaches. Boundary-based approaches detect corners on the boundaries of the objects. Gray-level approaches directly work on gray-level images by matching corner templates [40] or by computing gradients [59][76] at edge points. Kitchen and Rosenfeld [26] noted that gray-level schemes perform significantly better than binary techniques. Singh and Shneier [76] viewed the problem of gray-level corner detection as one similar to that of gray-level edge detection, and proposed a fusion method of template based techniques and gradient based techniques. Cooper *et al.* [9] used similarity between image patches along the edge direction, and showed that their method was more robust to noise than other gray corner detection methods including the Plessy, Kitchen-Rosenfeld and Beaudet [2] detectors. Zheng and *et al.* [87] proposed gradient-direction corner detector that is comparable to Plessy in detection but has better performance of localization and stability. Lee and Bien [32] developed a real-time gray-level corner detector using fuzzy logic and hardware implementation of the developed algorithm is studied to detect corners in real time.

Tsai, Hou and Su [81] proposed a boundary-based corner detection method based on the eigenvalues of the covariance matrix of data points on a curve segment. This is computationally fast and easy to implement. It avoids false alarms for superfluous corners and circular arcs. Laganiere [29] proposed a corner detector based on mathematical morphology. This approach is computationally very fast and yields results of good quality with suitable accuracy and robustness to noise. Lin, Chu and Hsueh [35] have proposed a modified morphological corner detector, which finds convex and concave significant points using simple integer computation. They use morphological operators to extract connected regions containing convex and concave corners. Then locate convex and concave corners as those points on the boundaries of the extracted region with maximal N-hit numbers. The drawbacks of this approach are:

(1) Difficult to choose a suitable structuring element to fit working purpose.

(2) As the size of structuring element increases, this method may increase the precision of the corners detected, but it will increase the computation as well.

2.3 Asymmetrical Closing for Corner Detection

Laganiere [29] proposed an approach to corner detection based on mathematical morphology. The goal of this approach was to obtain a fast corner detector that is, at the same time, sufficiently accurate, stable, selective and robust to noise.

Traditional opening and closing operators can be used for corner detection. The comparison of Figure 2.1(c) and (e) with (a) reveals the capability of opening and closing operators to detect corners when a cross-shaped structuring element is used. However, these corners suffer from the following problems.

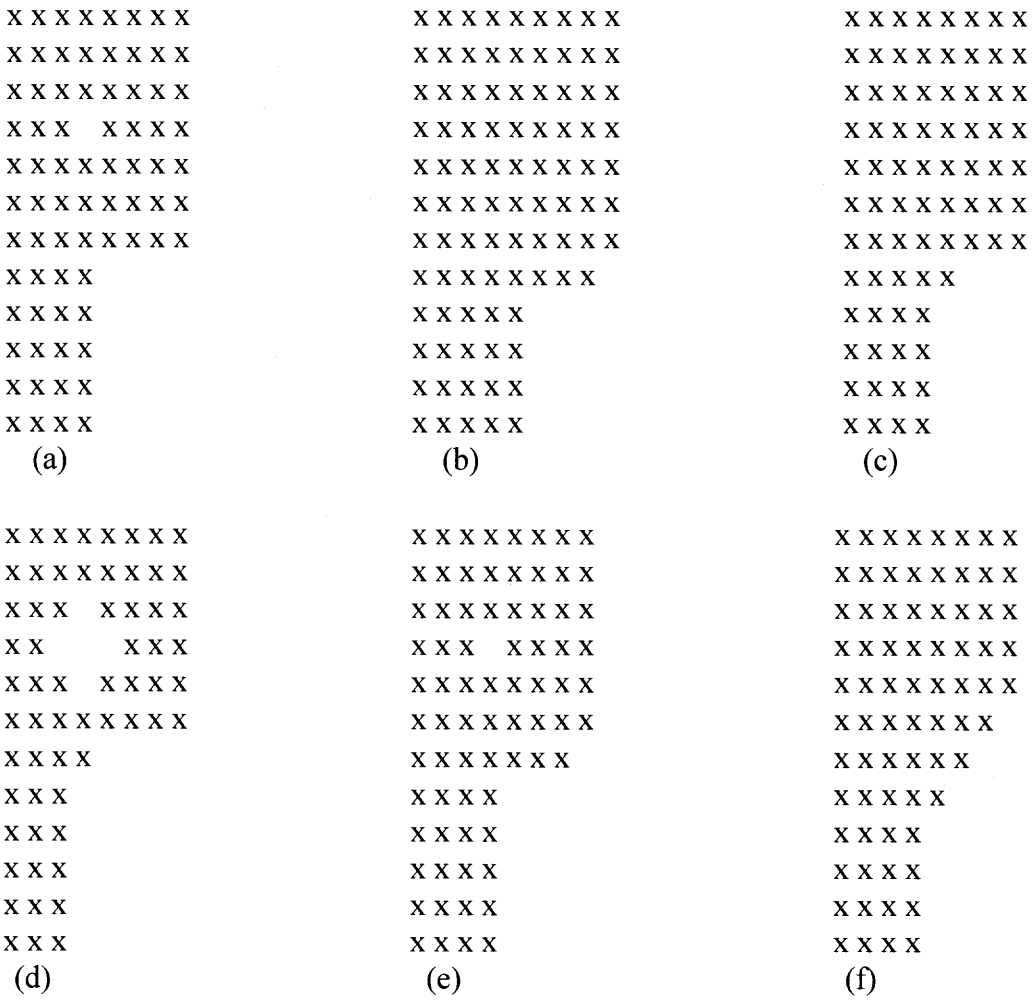

Figure 2.1 Opening and closing: (a) test pattern (b) erosion (c) opening (d) dilation (e) closing (f) asymmetrical closing.

1. Opening affects only the bright corners over dark background while closing affects only the dark corners over the bright background.
2. Small image structures are also eliminated and thus can be wrongly assimilated to corners.
3. This kind of corner detection is not rotationally invariant.

Laganiere proposed asymmetrical closing to overcome these problems. Asymmetrical closing is dilation of the image using a given structuring element followed

by an erosion using another structuring element. The central idea is to make dilation and erosion complementary in terms of the type of corners they affect. The structuring elements used are cross + as the first one and a lozenge ◊ for the second one. Asymmetrical closing of image A by structuring elements + and ◊ is given by

$$A^{c}_{+.\diamond} = (A \oplus +) \ominus \diamond \tag{2.1}$$

And corner strength is given by

$$C_{+}(A) = | A - A^{c}_{+.\diamond}| \tag{2.2}$$

This misses some corners and to detect those missing corners the following operator is used. (which is a 45° rotated version of the preceding one).

$$C_{\times}(A) = | A - A^{c}_{\times.\square}| \tag{2.3}$$

The combination of these two operators make corner detection almost rotationally invariant and insensitive to small image structures and leads to a the following operator,

$$C_{+.\times}(A) = | A^{c}_{+.\diamond} - A^{c}_{\times.\square}| \tag{2.4}$$

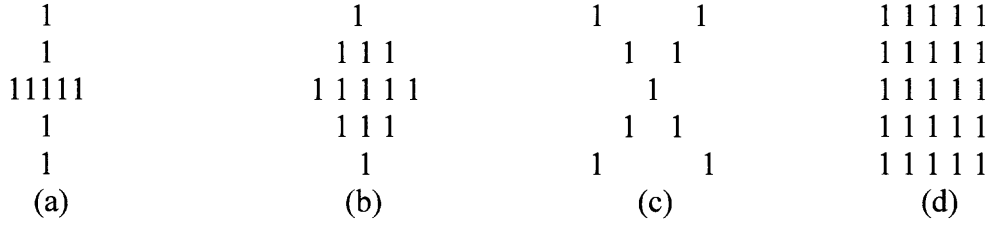

Figure 2.2 (a) Structuring element + (b) structuring element ◇ (c) structuring element × (d) structuring element □.

The operator proposed by Laganiere detects most of the corners. It does not detect wide-angle corners. Selecting median or center of a small neighborhood as the corner can reduce the multiple pixel response for some corners. Also it is found that in a binary like images where there are very dark objects in a bright background, taking the difference of

corner strengths of $A^c{}_{+,\diamond}$ and $A^c{}_{\times,\square}$ is removing some corners and taking the union of the strengths is a better option.

Some results of using this technique with the modification $C_{+,\times}(A) = | A - A^c{}_{+,\diamond} | \cup | A - A^c{}_{\times,\square}|$ instead of $C_{+,\times}(A) = | A^c{}_{+,\diamond} - A^c{}_{\times,\square}|$ are shown below.

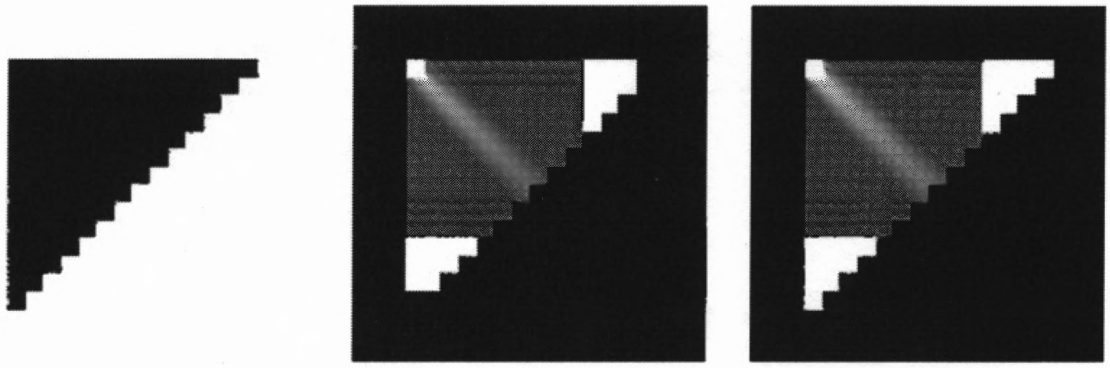

(a) (b) (c)

Figure 2.3 (a) Triangle binary image (b) Corners with Laganiere's operator (c) Corners with modified Laganiere's operator.

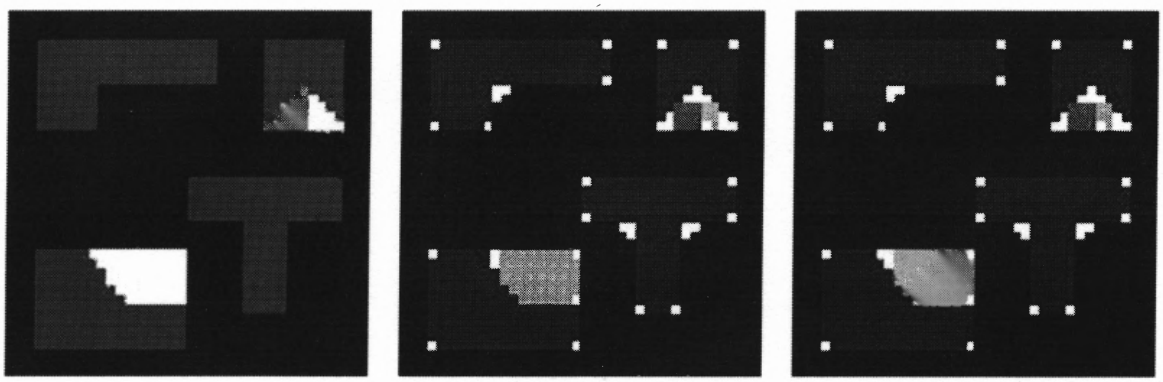

(a) (b) (c)

Figure 2.4 (a) Grayscale image (b) Corners with Laganiere's operator (c) Corners with modified Laganiere's operator.

2.4 Regulated Morphological Operations

The binary dilation collects shifts for which the kernel set intersects the object set without taking into account what is the size of the intersection, whereas the binary erosion collects shifts for which the kernel set is completely contained within the object set without considering shifts for which some kernel elements are not contained within the object set. As a result of these strict approaches, the ordinary morphological operations are sensitive to noise and small intrusions or protrusions on the boundary of shapes. In order to solve this problem, various extensions to the ordinary morphological operations have been proposed. These extensions can be classified into two major groups: fuzzy morphological operations [3][77] and soft morphological operations [28][71]. Agam and Dinstein [1] have defined regulated morphological operations, and shown how the fitting property of the ordinary morphological operations is controlled in these operations. The defined regulated morphological operations include: regulated erosion, regulated dilation, regulated open, and regulated close. The properties of the regulated morphological operations are discussed and it is shown that they posses many of the properties of the ordinary morphological operations. In particular, it is shown that the regulated open and close are idempotent for an arbitrary kernel and strictness parameter. Since the regulated morphological operations possess many of the properties of ordinary morphological operations, it is possible to use the regulated morphological operations in the existing algorithms that are based on morphological operations in order to improve their performance, where the strictness parameter of the regulated morphological operations may be optimized according to some criteria.

The following sections describe the regulated morphological operators as defined by Agam and Dinstein [1] and how these regulated dilation and erosion can be used for corner detection and show that this gives better results than that proposed by Laganiere [29] with less computation in case of binary images.

The *regulated dilation* of a set A by a set of structuring element B with a strictness of s is defined by:

$$A \oplus^{s} B = \{x \mid \#(A \cap (\hat{B})_x) \geq s\};\ s \in [1, \min(\#A, \#B)] \tag{2.5}$$

where the symbol # denotes the cardinality of a set.

The *regulated erosion* of set A by a set of structuring element B with a strictness of s is defined by:

$$A \ominus^{s} B = \{\, x \mid \#(A^{c} \cap (B)_x) < s\};\ s \in [1, \#B] \tag{2.6}$$

where the symbol # denotes the cardinality of a set.

Interested readers may refer [1] for more in detail regulated morphology and its properties.

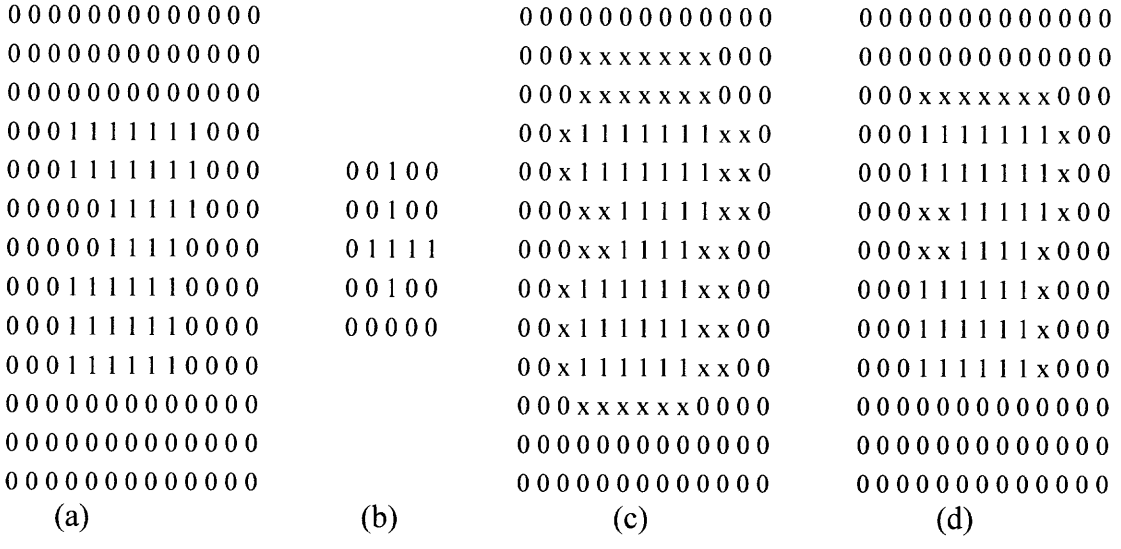

Figure 2.5 (a) Original shape (b) Structuring element (c) Ordinary dilation (d) Regulated dilation with a strictness of 2.

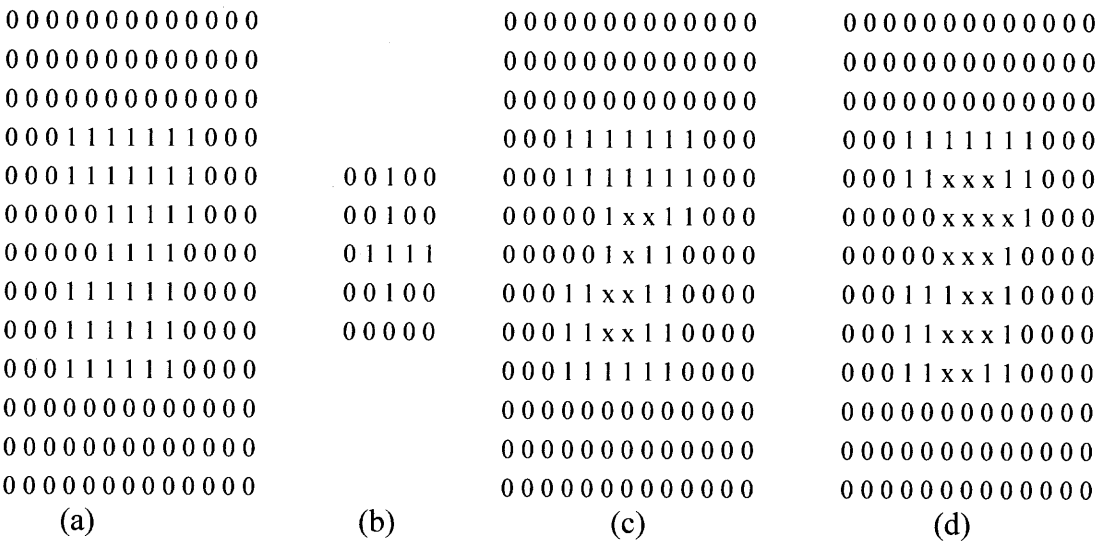

Figure 2.6 (a) Original shape (b) Structuring element (c) Ordinary erosion (d) Regulated erosion with a strictness of 2.

2.4.1 Regulated Morphological Operators for Corner Detection

For corner detection, the image is dilated with a 5×5 cross with a strictness of 2 followed by an erosion with the same structuring element with the same strictness. The resulting image A' is given by

$$A' = (A \oplus^s B) \ominus^s B \tag{2.7}$$

The corner strength will be given by comparing the resulting image with the original one,

$$C(A) = |A - A'| \tag{2.8}$$

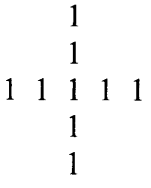

Figure 2.7 5×5 structuring element.

Corner detection with the above-discussed method uses only single structuring element for detecting as many corners detected by the operator proposed by Laganiere, which uses four different structuring elements. Some results of corner detection by regulated morphological closing are shown in Figure 2.8 - Figure 2.11. Figure 2.12 illustrates corner detection with different strictness values.

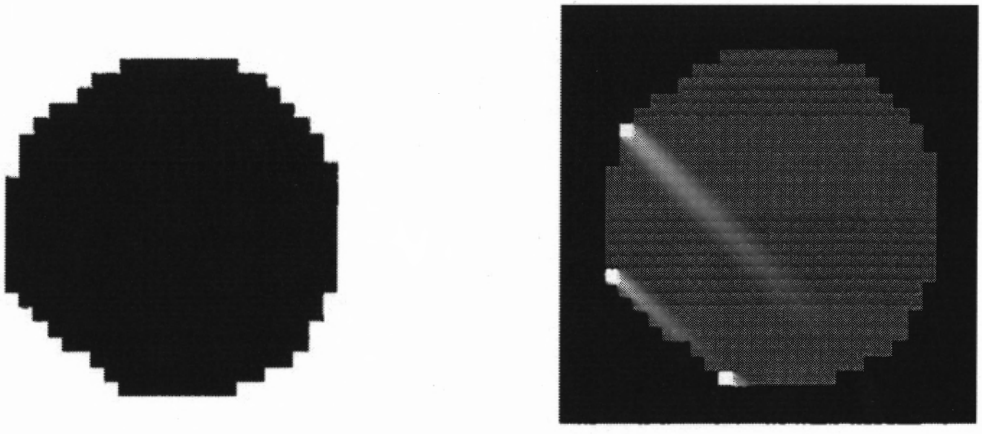

(a) (b)

Figure 2.8 (a) Circle (b) Corners with regulated closing with strictness 2.

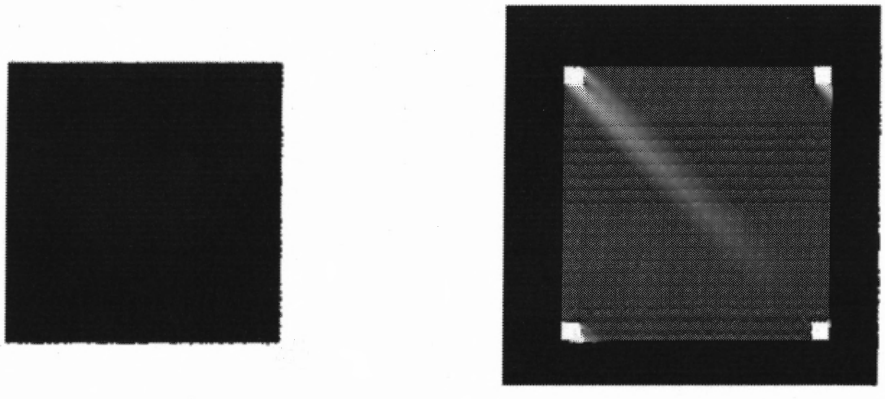

(a) (b)

Figure 2.9 (a) Square (b) Corners with regulated closing with strictness 2.

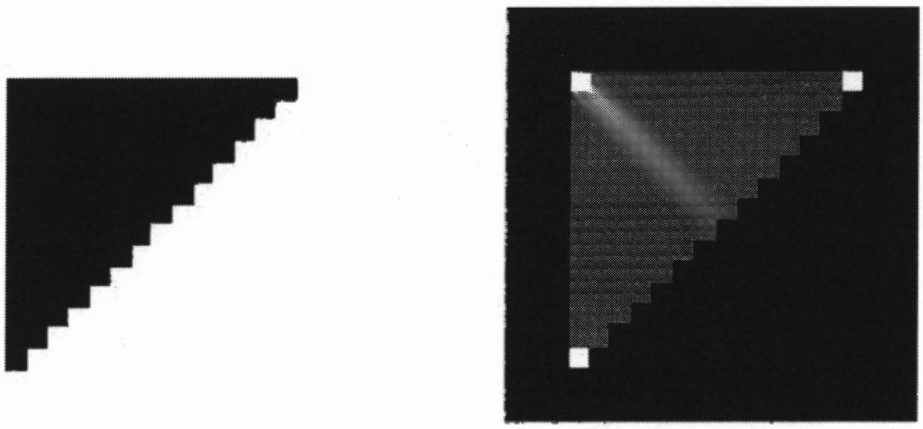

(a) (b)

Figure 2.10 (a) Triangle (b) Corners with regulated closing with strictness 2.

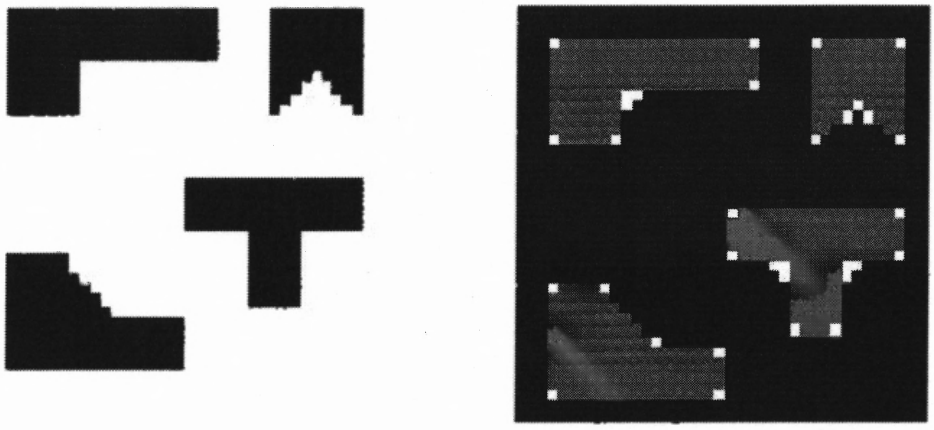

(a) (b)

Figure 2.11 (a) Image (b) Corners with regulated closing with strictness 2.

(a)

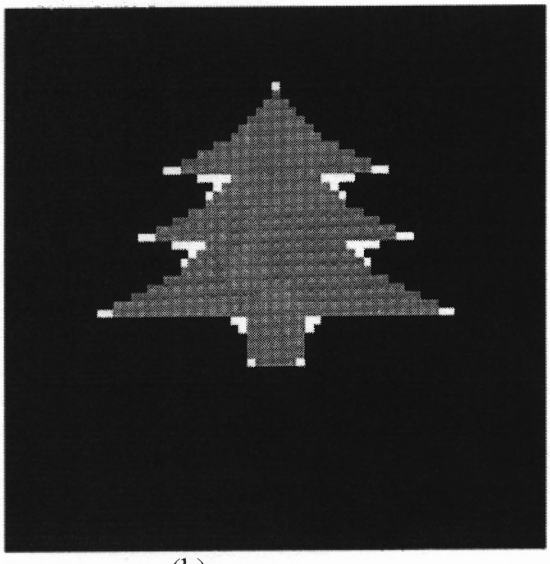

(b)

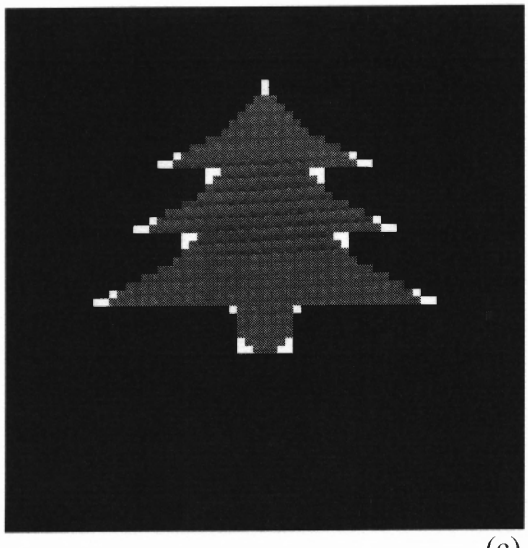

(c)

Figure 2.12 (a) Tree image (b)) Corners with regulated closing with strictness 2 (c) Corners with regulated closing with strictness 3.

2.5 Conclusions

It is shown that regulated morphological operations give better results for corner detection in binary images than Laganiere's method. Also it was shown that there is substantial reduction in computation as this uses one structuring element where as Laganiere method uses four structuring elements. Future work involves extending corner

detection using regulated morphology to grayscale images. One way of extending this is to compose the grayscale equivalents of the binary operations by processing thresholded sections of grayscale image by the binary operations, and then stacking the processed sections in order to obtain the grayscale result. Other areas of study are using fuzzy methods and ordered-statistics for corner detection directly on grayscale images.

CHAPTER 3

GENERAL SWEEP MATHEMATICAL MORPHOLOGY

General sweep mathematical morphology provides a new class of morphological operations, which allow one to select varying shapes and orientations of structuring elements during the sweeping process. Such a class holds syntactic characteristics similar to algebraic morphology as well as sweep geometric modeling. The conventional morphology is a subclass of the general sweep morphology. The sweep morphological dilation/erosion provides a natural representation of sweep motion in the manufacturing processes, and the sweep opening/closing provides variant degrees of smoothing in image filtering. The theoretical framework for representation, computation and analysis of sweep morphology is presented in this chapter. Its applications to the sweeping with deformations, image enhancement, edge linking, and shortest path planning for rotating objects are also discussed.

3.1 Introduction

The *sweep* operation to generate a new object by sweeping an object along a space curve trajectory provides a natural design tool in solid modeling. The simplest sweep is *linear extrusion* defined by a 2-D area swept along a linear path normal to the plane of the area to create a volume [54]. Another simple sweep is *rotational sweep* defined by rotating a 2-D object about an axis. Though simple, these two sweeps are often seen in real applications. Sweeps that generate area or volume changes in size, shape, or orientation during the sweeping process, and follow an arbitrarily curved trajectory are called *general sweeps* [16][53].

General sweeps of solids are useful in modeling the region swept out by a machine-tool cutting head or a robot following a path. General sweeps of 2-D cross-sections are known as *generalized cylinders* in computer vision, and are usually modeled as parameterized 2-D cross-sections swept at right angles along an arbitrary curve. Being the simplest of general sweeps, generalized cylinders are somewhat easy to compute. However, general sweeps of solids are difficult to compute since the trajectory and object shape may make the sweep object self-intersect [16].

Mathematical morphology involves the geometric analysis of shapes and textures in images. Appropriately used, mathematical morphological operations tend to simplify image data presenting their essential shape characteristics and eliminating irrelevancies [21][63][68][70]. As the object recognition, feature extraction, and defect detection correlate directly with shape, it becomes apparent that mathematical morphology is the natural processing approach to deal with the machine vision recognition process and the visually guided robot problem.

The mathematical morphological operations can be thought of working with two images. Conceptually, the image being processed is referred to as the active image and the other image being a kernel is referred to as the structuring element. Each structuring element has a designed shape, which can be thought of as a probe or filter of the active image. The active image can be modified by probing it with various structuring elements.

The two fundamental mathematical morphological operations are dilation and erosion. Dilation combines two sets using vector addition of set elements. Dilation by disk structuring elements corresponds to isotropic expansion algorithm popular to binary image processing. Dilation by small square (3×3) is an 8-neighborhood operation which

can be easily implemented by adjacently connected array architectures and is the one known by the name "fill," "expand," or "grow." Erosion is the morphological dual to dilation. It combines two sets using vector subtraction of set elements. Some equivalent terms of erosion are "shrink" and "reduce."

The traditional morphological operations perform vector additions or subtractions by a translation of structuring element to the object pixel. They are far from being capable of modeling the swept volumes of structuring elements moving with complex, simultaneous translation, scaling, and rotation in Euclidean space. In this chapter, an approach is developed that adopts sweep morphological operations to study the properties of swept volumes. The author presents the theoretical framework for representation, computation, and analysis of a new class of general sweep mathematical morphology and its practical applications. This chapter is organized as follows. Section 2 presents the theoretical development of general sweep mathematical morphology along with its properties. Section 3 describes an application of sweep morphology, which represents the blending of swept surfaces with deformations. Section 4 presents the usage of sweep morphology for image enhancement and Section 5 the edge linking and Section 6 the shortest path planning. The conclusions are made in Section 7.

3.2 Theoretical Development of General Sweep Mathematical Morphology

Traditional morphological dilation and erosion perform vector additions or subtractions by translating a structuring element along an object. These operations obviously have the limitation of orientation-dependence and can represent the sweep motion, which involves only translation. By including not only translation but also rotation and scaling, the entire theoretical framework and practical applications become extremely fruitful. Sweep

morphological dilation and erosion describe a motion of a structuring element that sweeps along the boundary of an object or an arbitrary curve by geometric transformations. The rotation angles and scaling factors are defined with respect to the boundary or the curve.

3.2.1 The Computation of Traditional Morphology

Because rotation and scaling are inherently defined on each pixel of the curve, the traditional morphological operations of an object by a structuring element need to be converted to the sweep morphological operations of a boundary by the structuring element. It is assumed throughout this chapter that the sets considered are connected and bounded.

Definition 1: *A* set S is said to be *connected* if each pair of points, $p, q \in S$ can be joined by a path which consists of pixels entirely located in S.

Definition 2: Given a set S, a *boundary* ∂S is defined as the set of points all of whose neighborhoods intersect both S and its complement S^c.

Definition 3: If a set S is connected and has no holes, it is called *simply connected*; if it is connected but has holes, it is called *multiply connected.*

Definition 4: Given a set S, the *outer boundary* $\partial_+ S$ of the set is defined as the closed loop of points in S that contains every other closed loop consisting of points of the set S; the *inner boundary* ∂S is defined as the closed loop of points in S that does not contain any other closed loop in S [84].

Proposition 1: If a set S is simply connected, then ∂S is its boundary; if it is multiply connected, then $\partial S = \partial_+ S \cup \partial_- S$.

Definition 5: The *positive filling* of a set S is denoted as $[S]_+$ and is defined as the set of all points that are inside the outer boundary of S; the *negative filling* is denoted as $[S]_-$ and is defined as the set of all points that are outside the inner boundary.

Note that if S is simply connected, then $[S]_-$ is a universal set. Therefore, no matter what S is simply or multiply connected, $S = [S]_+ \cap [S]_-$.

Proposition 2: Let A and B be simply connected sets. The dilation of A by B equals the positive filling of $\partial A \oplus B$, i.e., $A \oplus B = [\partial A \oplus B]_+$. The significance is that if A and B are simply connected sets, then just compute the dilation of the boundary ∂A by the set B. This leads to a substantial reduction of computation.

Proposition 3: If A and B are simply connected sets, the dilation of A by B equals the positive filling of the dilation of their boundaries, i.e., $A \oplus B = [\partial A \oplus \partial B]_+$.

This proposition reduces further the computation required for the dilation. Namely, the dilation of sets A by B can be computed by the dilation of the boundary of A by the boundary of B.

Proposition 4: If A is multiply connected and B is simply connected, $A \oplus B = [\partial_+ A \oplus \partial B]_+ \cap [\partial_- A \oplus \partial B]_-$.

Since A and B possess the commutative property with respect to dilation, the following proposition can be easily obtained.

Proposition 5: If A is simply connected and B is multiply connected, $A \oplus B = [\partial A \oplus \partial_+ B]_+ \cap [\partial A \oplus \partial_- B]_-$.

3.2.2 The General Sweep Mathematical Morphology

The sweep morphology can be represented as a 4-tuple, $\Psi(B, A, S, \Theta)$, where B is a structuring element set, indicating a primitive object; A is either a curve path or a closed object whose boundary representing the sweep trajectory with a parameter t along which the structuring element B is swept; $S(t)$ is a vector consisting of the scaling factors; $\Theta(t)$ is a vector consisting of the rotation angles. Note that both scaling factors and rotation angles are defined with respect to the sweep trajectory.

Definition 6: If A is a simply connected object and let ∂A denote its boundary, the *sweep morphological dilation* of A by B in Euclidean space is denoted by $A \boxplus B$ and is defined as

$$A \boxplus B = \{c \mid c = a + b \text{ for some } a \in A \text{ and } b \in [B \times S(t) \times \Theta(t)\ ]\}.$$

This is equivalent to performing on the boundary of A (i.e., ∂A) and taking the positive filling as

$$A \boxplus B = \{\cup_{0 \le t \le 1} \cup_{b \in B} [\partial A(t) + b \times S(t) \times \Theta(t)]\}_+.$$

If A is a curve path, i.e., ∂A = A, the sweep morphological dilation of A by B is defined as

$$A \boxplus B = \cup_{0 \le t \le 1} \cup_{b \in B} [A(t) + b \times S(t) \times \Theta(t)].$$

Note that if B does not involve rotations (or B is rotation-invariant like a circle) and scaling, then the sweep dilation is equivalent to the traditional morphological dilation.

Figure 3.1(a) shows a curve and Figure 3.1(b) shows an elliptical structuring element. The rotation angle θ is defined as $\theta(t) = \tan^{-1} (dy/dt)/(dx/dt)$ along the curve with parameter t in the range of [0,1]. The traditional morphological dilation is shown in Figure 3.1(c) and the sweep dilation using the defined rotation is shown in Figure 3.1(d).

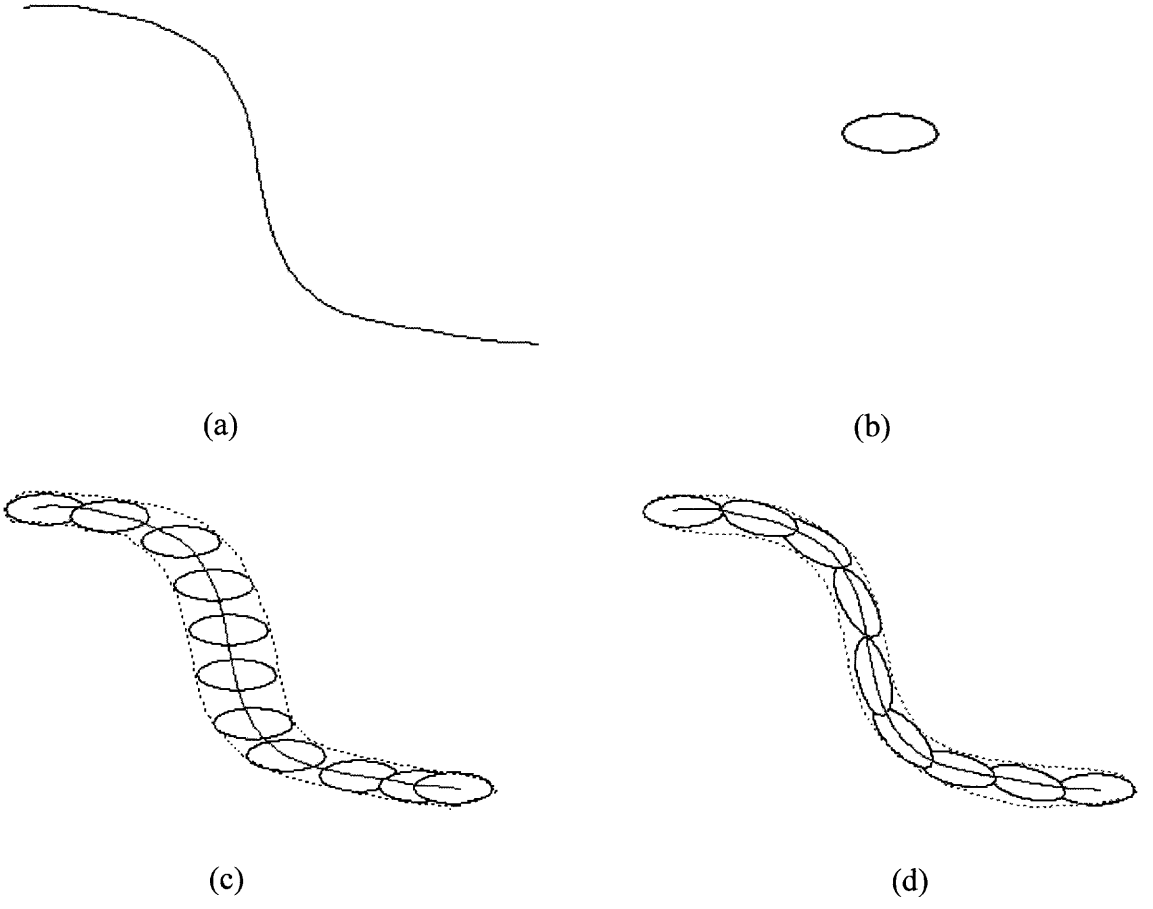

Figure 3.1 (a) An open curve path, (b) a structuring element, (c) result of a traditional morphological dilation, (d) result of a sweep morphological dilation.

A geometric transformation of the structuring element specifies the new coordinates of each point as functions of the old coordinates. Note that the new coordinates are not necessarily integers after a transformation to a digital image is applied. To make the results of the transformation into a digital image, they must be resampled or interpolated. Since a two-valued (black-and-white) image is being transformed, the zero-order interpolation is adopted.

The sweep morphological erosion, unlike dilation, is defined with the restriction on a closed object only and its boundary represents the sweep trajectory.

Definition 7: Let A be a closed object and B be a structuring element. The *sweep morphological erosion* of A by B in Euclidean space, denoted by $A \boxminus B$, is defined as

$$A \boxminus B = \{c \mid c + b \in A \text{ and for every } b \in [B \times S(t) \times \Theta(t)] \}.$$

An example of a sweep erosion by an elliptical structuring element whose semi-major axis is tangent to the boundary is shown in Figure 3.2. Like in traditional morphology, the general sweep morphological opening can be defined as a general sweep erosion of A by B followed by a general sweep dilation, where A must be a closed object. The sweep morphological closing can be defined in the opposite sequence, i.e., a general sweep dilation of A by B followed by a general sweep erosion, where A can be either a closed object or a curve path.

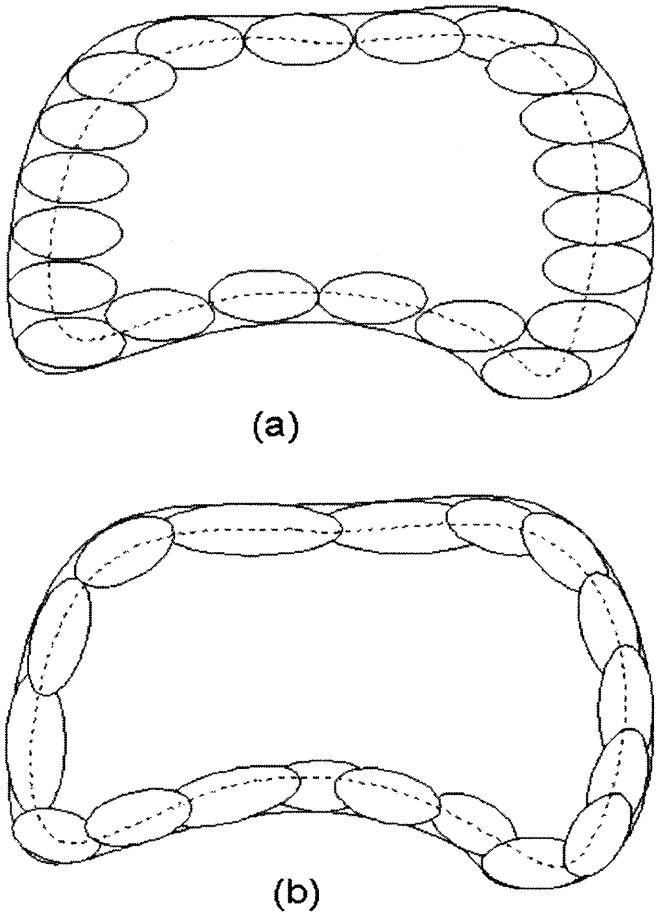

Figure 3.2 (a) Traditional erosion (b) sweep erosion.

The propositions of traditional morphological operations can be extended to sweep morphological operations.

Proposition 6: If the structuring element B is simply connected, the sweep dilation of A by B equals to the positive filling of the sweep dilation by the boundary of B, i.e.,

$A \boxplus B = [A \boxplus \partial B]_+$.

Extending this proposition to multiply connected objects, the following three cases are obtained.

Case 6(a): If A is multiply connected, i.e., $\partial A = \partial_+ A \cup \partial A$, then

$A \boxplus B = [\partial_+ A \boxplus B]_+ \cap [\partial A \boxplus B]_-$.

Case 6(b): If B is multiply connected, i.e., $\partial B = \partial_+ B \cup \partial B$, then

$A \boxplus B = [A \boxplus \partial_+ B]_+ \cap [A \boxplus \partial B]_-$.

Case 6(c): Finally, if both A and B are multiply connected, i.e., $\partial A = \partial_+ A \cup \partial A$ and $\partial B = \partial_+ B \cup \partial B$, then

$A \boxplus B = [(\partial_+ A \cup \partial A) \boxplus \partial_+ B]_+ \cap [(\partial_+ A \cup \partial A) \boxplus \partial B]_-$.

This leads to a substantial reduction of computation. An analogous development for the sweep erosion can be made.

Proposition 7: If A and B are simply connected sets, then $A \boxminus B = A \boxminus \partial B$.

With the aforementioned propositions and considering the boundary of the structuring element, the computation of sweep morphological operations can further be reduced.

3.2.3 The Properties of Sweep Morphological Operations

Property 1: Non-commutative. Because of the rotational factor in the operation, the commutativity does not hold, i.e., $A \boxplus B \neq B \boxplus A$.

Property 2: Non-associative. Because the rotational and scaling factors are dependent on the characteristics of the boundary of the object, associativity does not hold. Hence, $A \boxplus (B \boxplus C) \neq (A \boxplus B) \boxplus C$.

But associativity of regular dilation and sweep dilation holds, i.e., $A \oplus (B \boxplus C) = (A \oplus B) \boxplus C$. As structuring element is rotated based on the boundary properties of B and after $A \oplus B$, still the boundary properties will be similar to that of B.

Property 3: Translational Invariance:

$$\begin{aligned} A_x \boxplus B &= [\cup_{0\le t\le 1} \cup_{b\in B} [\partial A + x + b \times S(t) \times \theta(t)]]_+ \\ &= [\cup_{0\le t\le 1} \cup_{b\in B} [\partial A + b \times S(t) \times \theta(t)] + x]_+ \\ &= [\cup_{0\le t\le 1} \cup_{b\in B} [\partial A + b \times S(t) \times \theta(t)]]_+ + x \\ &= (A \boxplus B)_x. \end{aligned}$$

Sweep erosion can be derived similarly.

Property 4: Increasing property will not hold in general. If the boundary is smooth, i.e., derivative exists everywhere, then increasing property will hold.

Property 5: Distributivity

(a) *Distributivity over union.* Dilation is distributive over union of structuring elements. That is, dilation of A with a union of two structuring elements B and C is the same as union of dilation of A with B and dilation of A with C.

$$\begin{aligned} A \boxplus (B \cup C) &= [\cup_{0\le t\le 1} \cup_{b\in B\cup C} [\partial A + b \times S(t) \times \theta(t)]]_+ \\ &= [\cup_{0\le t\le 1} [\cup_{b\in B} [\partial A + b \times S(t) \times \theta(t)] \cup \\ &\qquad \cup_{b\in C} [\partial A + b \times S(t) \times \theta(t)]]]_+ \\ &= [[\cup_{0\le t\le 1} \cup_{b\in B} [\partial A + b \times S(t) \times \theta(t)]] \cup \\ &\quad [\cup_{0\le t\le 1} \cup_{b\in C} [\partial A + b \times S(t) \times \theta(t)]]]_+ \\ &= [\cup_{0\le t\le 1} \cup_{b\in B} [\partial A + b \times S(t) \times \theta(t)]]_+ \cup \\ &\quad [\cup_{0\le t\le 1} \cup_{b\in C} [\partial A + b \times S(t) \times \theta(t)]]_+ \\ &= (A \boxplus B) \cup (A \boxplus C). \end{aligned}$$

(b) Dilation is not distributive over union of sets. That is, dilation of $(A \cup C)$ with a structuring element B is not same as union of dilation of A with B and dilation of C with B.

$(A \cup C) \boxplus B \neq (A \boxplus B) \cup (C \boxplus B)$.

(c) Erosion is anti-distributive over union of structuring elements. That is, erosion of A with a union of two structuring elements B and C is the same as intersection of erosion of A with B and erosion of A with C.

(d) *Distributivity over intersection.*

$\partial A \boxplus (B \cap C) = [\cup_{0 \le t \le 1} [\cup_{b \in B \cap C} [\partial A + b \times S(t) \times \theta(t)]]$

$\Rightarrow \partial A \boxplus (B \cap C) \subseteq [\cup_{0 \le t \le 1} [\cup_{b \in B} [\partial A + b \times S(t) \times \theta(t)]]$

and also

$\partial A \boxplus (B \cap C) \subseteq [\cup_{0 \le t \le 1} [\cup_{b \in C} [\partial A + b \times S(t) \times \theta(t)]]$.

Therefore,

$\partial A \boxplus (B \cap C) \subseteq (\partial A \boxplus B) \cap (\partial A \boxplus C)$

which implies,

$[\partial A \boxplus (B \cap C)]_+ \subseteq [(\partial A \boxplus B)]_+ \cap [(\partial A \boxplus C)]_+$

i.e.,

$A \boxplus (B \cap C) \subseteq (A \boxplus B) \cap (A \boxplus C)$.

3.3 Blending of Swept Surfaces with Deformations

By using the general sweep mathematical morphology, a smooth sculptured surface can be described as a trajectory of cross-section curve swept along a profile curve, where the trajectory of cross-section curve is the structuring element B and the profile curve is the open or closed curve C. It is very easy to describe the sculptured surface by specifying the 2-D cross-sections, and that the resulting surface is aesthetically appealing. The designer can envision the surface as a blended trajectory of cross-section curves swept along a profile curve.

Let ∂B denote the boundary of a structuring element B. A swept surface $S_w(\partial B, C)$ is produced by moving ∂B along a given trajectory curve C. The plane of B must be perpendicular to C at any time instance. The contour curve is represented as a B-spline curve and ∂B is represented as the polygon net of the actual curve. This polygon net is swept along the trajectory to get the intermediate polygon nets and later they are interpolated by a B-spline surface. Twisting or scaling uniformly or by applying the deformations to selected points of ∂B can deform the curve. The curve can also be deformed by varying the weights at each of the points. When a uniform variation is desired, it can be applied to all the points and otherwise to some selected points. These deformations are applied to ∂B before it is moved along the trajectory C.

Let ∂B denote a planar polygon with n points and each point $\partial B_i = (x_i, y_i, z_i, h_i)$, where $i = 1, 2, ..., n$. Let C denote any 3-D curve with m points and each point $C_j = (x_j, y_j, z_j)$, where $j = 1, 2, ...,m$. The scaling factor, weight, and twisting factor for point j of C are denoted as sx_j, sy_j, sz_j, w_j, and θ_j, respectively. The deformation matrix is obtained as $[S_d] = [S_{sw}][R_\theta]$, where

$$[S_{sw}]=\begin{bmatrix} sx_j & 0 & 0 & 0 \\ 0 & sy_j & 0 & 0 \\ 0 & 0 & sz_j & 0 \\ 0 & 0 & 0 & w_j \end{bmatrix}$$

and

$$[R_\theta]=\begin{bmatrix} \cos\theta_j & \sin\theta_j & 0 & 0 \\ -\sin\theta_j & \cos\theta_j & 0 & 0 \\ 0 & 0 & 1 & 0 \\ 0 & 0 & 0 & 1 \end{bmatrix}.$$

The deformed ∂B must be rotated in 3-D with respect to the tangent vector at each point of trajectory curve C. To calculate the tangent vector, two points C_0 and C_{m+1} are added to C, where $C_0 = C_1$ and $C_{m+1} = C_m$. The rotation matrix R_x about x-axis is given by

$$[R_x]=\begin{bmatrix} 1 & 0 & 0 & 0 \\ 0 & \cos\alpha_j & \sin\alpha_j & 0 \\ 0 & -\sin\alpha_j & \cos\alpha_j & 0 \\ 0 & 0 & 0 & 1 \end{bmatrix}, \text{ where}$$

$$\cos\alpha_j = \frac{cy_{j-1} - cy_{j+1}}{h_x}, \quad \sin\alpha_j = \frac{cz_{j+1} - cz_{j-1}}{h_x},$$

$$h_x = \sqrt{(cy_{j-1} - cy_{j+1})^2 + (cz_{j+1} - cz_{j-1})^2}.$$

The rotation matrices about y- and z-axes can similarly be derived. Finally, ∂B must be translated to each point of C and the translation matrix C_{xyz} is given by

$$[C_{xyz}]=\begin{bmatrix} 1 & 0 & 0 & 0 \\ 0 & 1 & 0 & 0 \\ 0 & 0 & 1 & 0 \\ Cx_j - Cx_1 & Cy_j - Cy_1 & Cz_j - Cz_1 & 1 \end{bmatrix}.$$

The polygon net of the sweep surface will be obtained by $[B_{i,j}] = [\partial B_i]\ [S_d]\ [Sw_C]$, where $[Sw_C] = [R_x]\ [R_y]\ [R_z][C_{xyz}]$.

The B-spline surface can be obtained from the polygon net by finding the B-spline curve at each point of C. To get the whole swept surface, the B-spline curves at each point of the trajectory C have to be calculated. Selecting a few polygon nets and calculating the B-spline surface can reduce this computation.

Example 1: Sweeping of a square along a trajectory with deformation to a circle.

Here the deformation is only the variation of the weights. The circle is represented as a rational B-spline curve. The polygon net is a square with 9 points with the first and last being the same and the weights of the corner vary from 5 to $\sqrt{2}/2$ as it is being swept along the trajectory C, which is given in the parametric form as $x = 10s$ and $y = \cos(\pi s)$ - 1. The sweep transformation is given by

$$[Sw_T] = \begin{bmatrix} \cos\psi & \sin\psi & 0 & 0 \\ -\sin\psi & \cos\psi & 0 & 0 \\ 0 & 0 & 1 & 0 \\ 10s & \cos\pi s & 0 & 1 \end{bmatrix} \text{ where } \psi = \tan^{-1}\left(\frac{-\pi \sin(\pi s)}{10}\right).$$

Figure 3.3 shows the sweeping of a square along a trajectory with deformation to a circle.

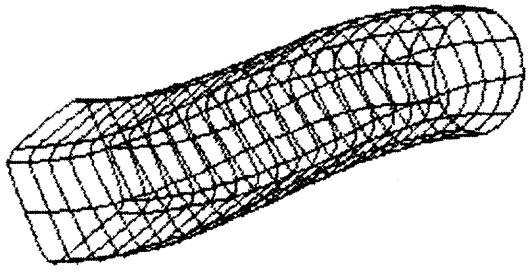

Figure 3.3 Sweeping of a square along a trajectory with deformation to a circle.

3.4 Image Enhancement

Because of being adapted to local properties of the image, general sweep morphological operations can provide variant degrees of smoothing for noise removal while preserving the object features. Research on statistical analysis of traditional morphological operations has been found. Stevenson and Arce [80] developed the output distribution function of opening with flat structuring elements by threshold decomposition. Morales and Acharya [41] presented general solutions for the statistical analysis of morphological openings with compact, convex, and homothetic structuring elements.

Traditional opening can remove noise as well as object features whose sizes are smaller than the structuring element. With the general sweep morphological opening, the object features of similar shape and greater size compared to the structuring element will be preserved while removing noise. In general, the highly varying parts of the image are assigned with smaller structuring elements, while the slowly varying parts with larger ones. The structuring elements can be assigned based on the contour gradient variation.

An example is illustrated in Figure 3.4, (a) circular structuring element scaled based on the gradient of the signal and (b) elliptical structuring element rotated based on the slope and scaled based on the curvature of the signal.

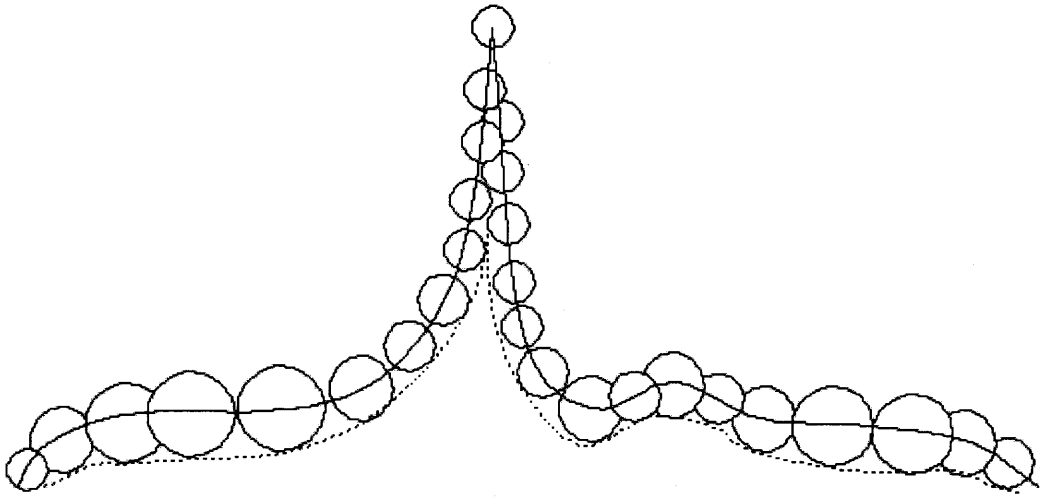

(a)

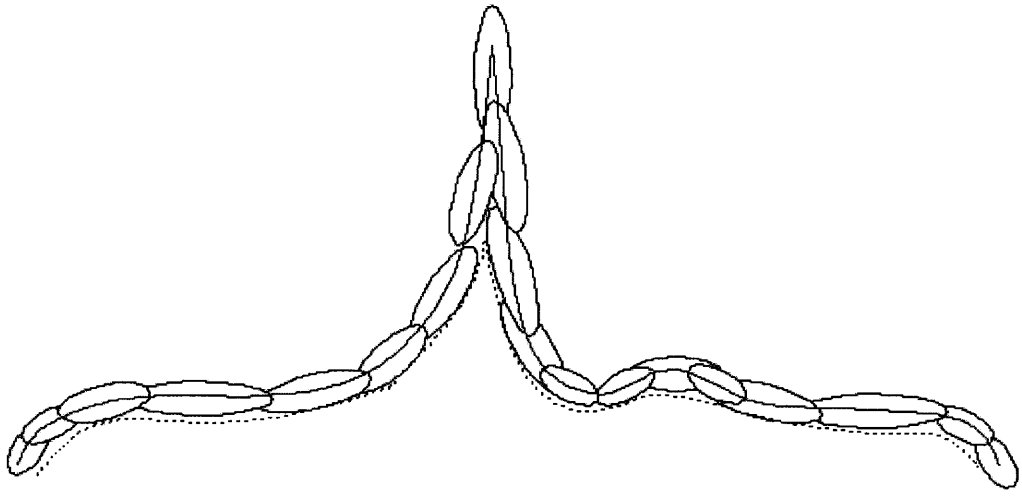

(b)

Figure 3.4 Structuring element assignment using general sweep morphology.

Step edge is an important feature in an image. Assume a noisy step edge is defined as

$$f(x) = \begin{cases} N_x & if\ x < 0 \\ h + N_x & if\ x \geq 0 \end{cases}$$

where h is the strength of the edge, and N_x is i.i.d. Gaussian random noise with mean value 0 and variance 1. For image filtering with a general sweep morphological opening, essentially adopt smaller sized structuring element for the important feature points, and larger one for other locations. Therefore, the noise in an image is removed while the features are preserved. For instance, in a one-dimensional image, it can be easily achieved by computing the gradient by $f(x) - f(x-1)$ and setting those points accordingly, in which the gradient values are larger than the predefined threshold, with smaller structuring elements.

Chen and *et al.* [6] presented the results of noisy step edge filtering by both traditional morphological opening and so-called *space-varying* (involving both scaling and translation in the general sweep morphology model) opening and compared by computing the mean and variance of output signals. The mean value of the output distribution follows the main shape of the filtering result well and this gives the evidence of shape preserving ability of the proposed operation. Meanwhile, the variance of output distribution coincides with the noise variance, and this shows the corresponding noise removal ability. It is observed that general sweep opening possesses approximately the same noise removing ability as compared to the traditional one. Moreover, it can be observed that, the relative edge strength with respect to the variation between the transition interval, say [-2,2], for general sweep opening, is larger than that of the traditional one. This explains why the edge is degraded in the traditional morphology case but is enhanced in the general sweep one. Although a step-edge model was tested successfully, other complicated cases need further elaboration. The statistical analysis for

providing a quantitative approach to general sweep morphological operations will be further investigated.

Chen and *et al.* [7] have shown image filtering using adaptive signal processing, which is nothing but the sweep morphology with only scaling and translation. The method uses space varying structuring elements by assigning different filtering scales to the feature parts and other parts. To adaptively assign structuring elements, they have developed the progressive umbra-filling (PUF) procedure. This is an iterative process. The experimental results have shown that this approach can successfully eliminate noise without over smoothing the important features of a signal.

3.5 Edge Linking

Edge is a local property of a pixel and its immediate neighborhood. Edge detector is a local processing to locate sharp changes in the intensity function. An ideal edge has a step like cross section as gray levels change abruptly across the border. In practice, edges in digital images are generally slightly blurred as effects of sampling and noise.

There are many edge detection algorithms and the basic idea underlying most edge detection techniques is the computation of a local derivative operator [20]. Some algorithms like the LoG filter produce closed edges, however, false edges are generated when blur and noise appear in an image. Some algorithms like Sobel operator produce noisy boundaries that do not actually lie on the borders and broken gaps where border pixels should reside. That is because noise and breaks present in the boundary from non-uniform illumination and other effects that introduce spurious intensity discontinuities. Thus, edge detection algorithms are typically followed by linking and other boundary

detection procedures, which are designed to assemble edge pixels into meaningful boundaries.

The edge linking by the tree search technique was proposed by Matelli [37] to link the edge sequentially along the boundary between pixels. The cost of each boundary element is defined by the step size between the pixels on its both sides. The larger the intensity difference corresponds to the larger the step size, which is assigned a lower cost. The path of boundary elements with the lowest cost is linked up as an edge. The cost function was later redefined by Cooper *et al.* [8], where the edge is extended through the path having a maximal local likelihood. Similar efforts were made by Eichel and Delp [14] and by Farag and Edward [15].

Basically, the tree search method is time-consuming and requires the suitable assignment of root points. Another method locates all of the ends points of the broken edges and uses a relaxation method to pair them up, so that line direction is maintained, lines are not allowed to cross, and closer points are matched first. However, this suffers problems if unmatched end points or noises are present.

A simple approach to edge linking is a morphological dilation of points by some arbitrarily selected radius of circles followed by the OR operator of the boundary image with the resulting dilated circles and the result is finally skeletonized [62]. This method, however, has the problem that some of the points may be too far apart for the circles to touch, while oppositely the circles may obscure details by touching several existing lines. To overcome this, the sweep mathematical morphology is used to allow the variation of the structuring element according to local properties of the input pixels.

3.5.1 Edge Linking using Sweep Morphology

Let B denote an elliptic structuring element shown in Figure 3.5, where p and q denote respectively the semi-major and semi-minor axes. That is

$$\partial B \equiv \{ [x,y]^T \mid x^2/p^2 + y^2/q^2 = 1 \}. \tag{3.1}$$

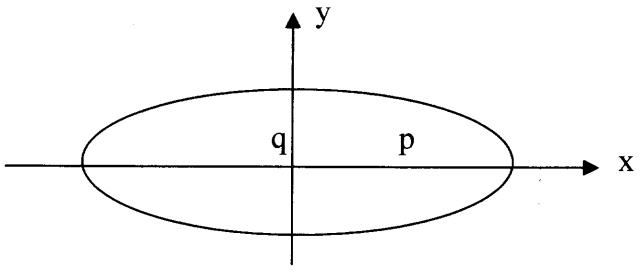

Figure 3.5 The elliptic structuring element.

An edge-linking algorithm was proposed by Shih and Cheng based on the sweep dilation, thinning and pruning [65]. This is a three-step process as explained below.

Step 1: Sweep Dilation.

The broken line segments can be linked up by using the sweep morphology provided that the structuring element is suitably adjusted. Considering the input signal plotted in Figure 3.6(a), the concept of using the sweep morphological dilation is illustrated in Figure 3.6(b). Extending the line segments in the direction of local slope performs the linking. The basic shape of the structuring element is an ellipse, where the major axis is always aligned with the tangent of the signal.

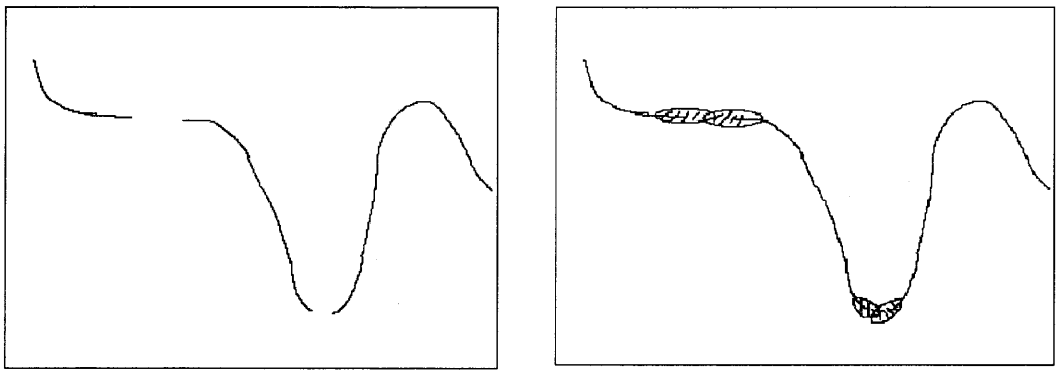

(a) (b)

Figure 3.6 (a) Input signal (b) Sweep dilation with elliptical structuring elements.

Elliptical structuring element is to reduce noisy edge points and small insignificant branches. The width of the ellipse is selected to accomplish this purpose. The major axis of the ellipse should be adapted to the local curvature of the input signal to protect from over stretch at high curvature point. At high curvature points, a short major axis is selected and vice versa.

Step 2: Thinning.

After performing the sweep dilation by directional ellipses, the edge segments are extended in the direction of the local slope. Because the tolerance (or the minor axis of the ellipse) is added, the edge segments grow a little fat. To suppress this effect, morphological thinning is adopted.

An algorithm of thinning using mathematical morphology is proposed by Jang and Chin [24]. The skeletons generated by their algorithm are connected, one pixel width, and closely follow the medial axes. The algorithm is an iterative process based on the hit/miss operation. Four structuring elements are constructed to remove boundary pixels from four directions, and another four are constructed for removing the extra pixels at skeleton junctions. There are four passes in each iteration. Three of the eight predefined

structuring elements templates are applied simultaneously in each pass. The iterative process is performed until the result converges. The thinning algorithm will not shorten the skeletal legs. Therefore, it is applied to the adaptive dilated edges.

Step 3: Pruning:

The dilated edge segments after thinning may still produce a small number of short skeletal branches. These short branches should be pruned. In a skeleton, any pixel, which has three or more neighbors, is called a root. Starting from each neighbor of the root pixel, the skeleton is traced outward. Those paths whose lengths are shorter than a given threshold k are treated as branches and are pruned away.

Figure 3.7(a) shows an original elliptical edge and Figure 3.7(b) shows its randomly discontinuous edge. The sweep morphological edge-linking algorithm is experimented on Figure 3.7(b). Figure 3.8 shows the results of using circular structuring elements with radius r=3, r=5 and r=10, respectively, in 5 iterations. Compared with the original ellipse in Figure 3.7(a), it is known that if the gap is larger than the radius of the structuring element, it is difficult to link the gap smoothly. However, if a very big circular structuring element is used, the edge will look hollow and protuberant. Also, using big circle can obscure the details of edge.

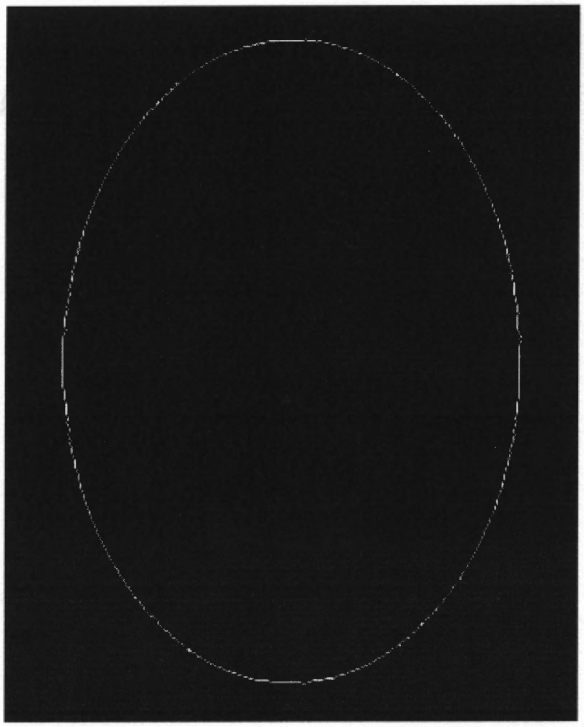

(a)

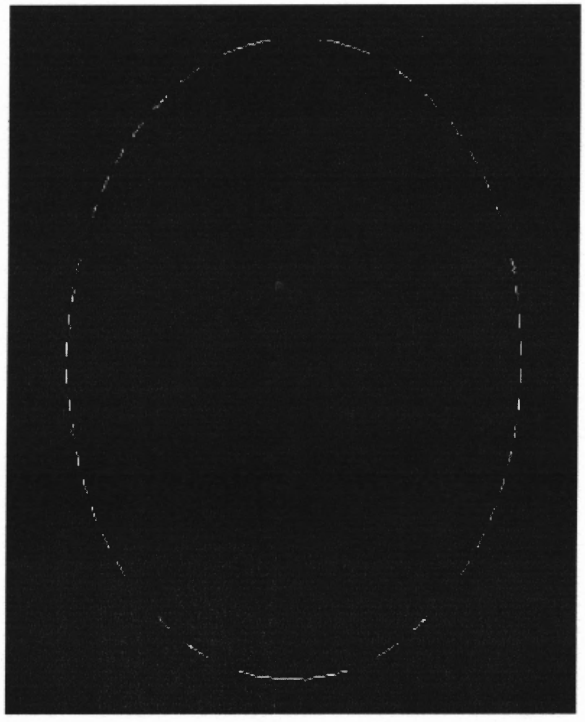

(b)

Figure 3.7 (a) Original elliptical edge and (b) Its randomly discontinuous edge.

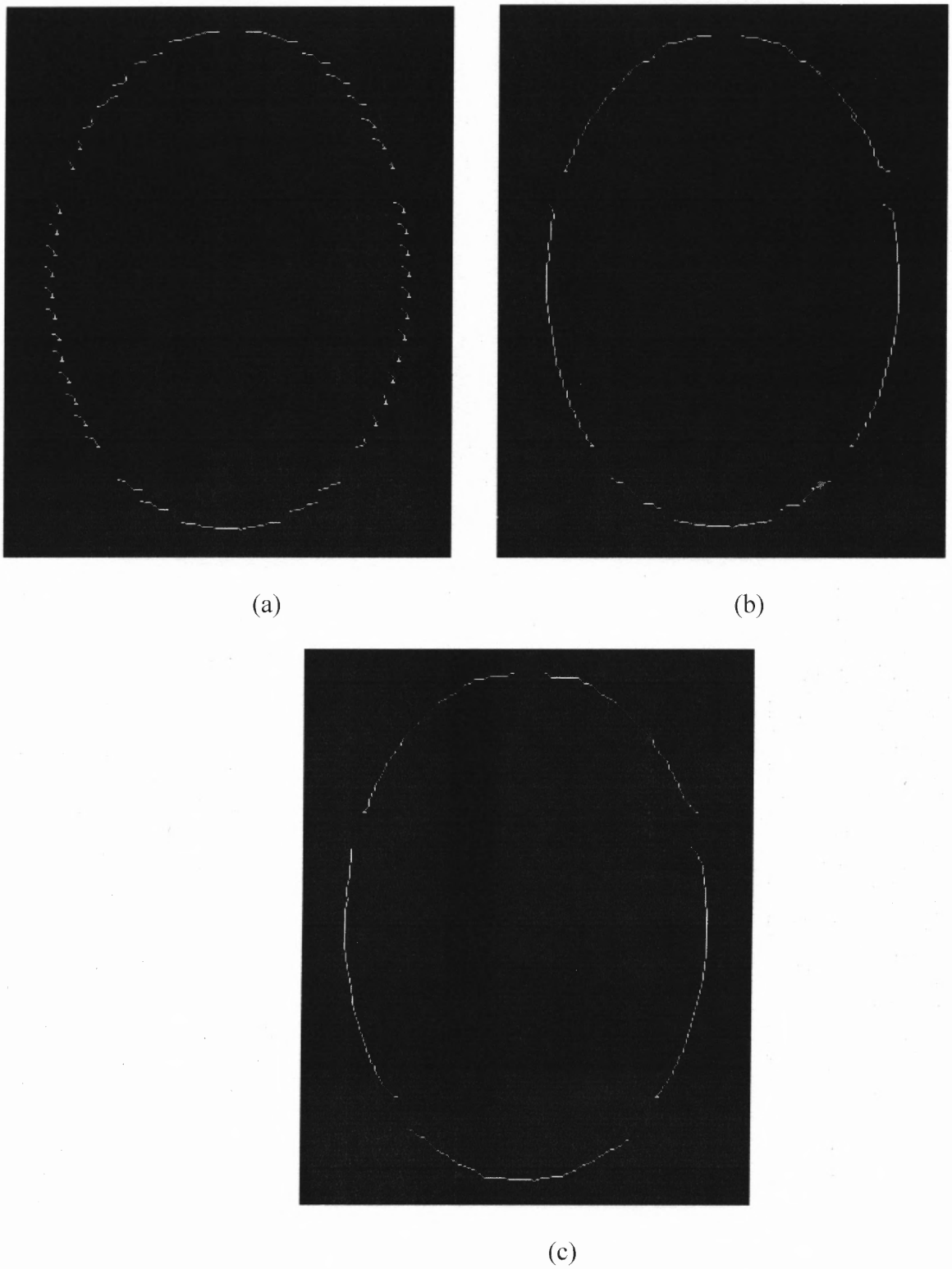

Figure 3.8 Using circular structuring elements in 5 iterations with (a) r=3, (b) r=5, and (c) r=10.

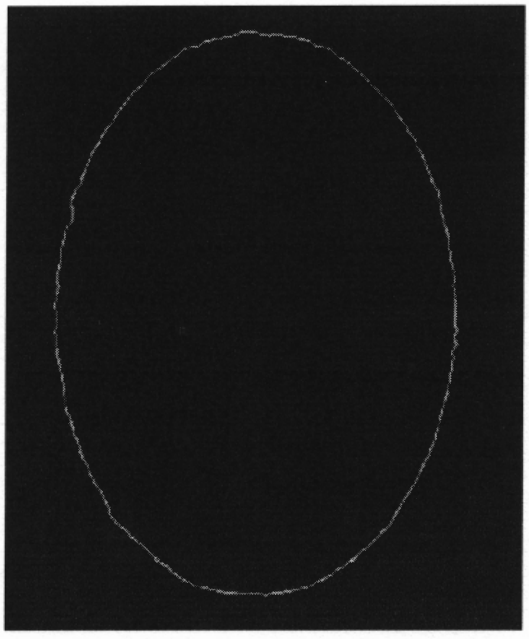

Figure 3.9 Using the sweep morphological edge-linking algorithm.

Figure 3.9 shows the result of using the sweep morphological edge-linking algorithm. Figure 3.10(a) shows the edge of an industrial part and Figure 3.10(b) shows its randomly discontinuous edge. Figure 3.10(c) shows the result of using the sweep morphological edge-linking algorithm. Figure 3.11(a) shows the edge with added uniform noise and Figure 3.11(b) shows the edge after removing noise. Figure 3.11(c) shows the result of using the sweep morphological edge-linking algorithm.

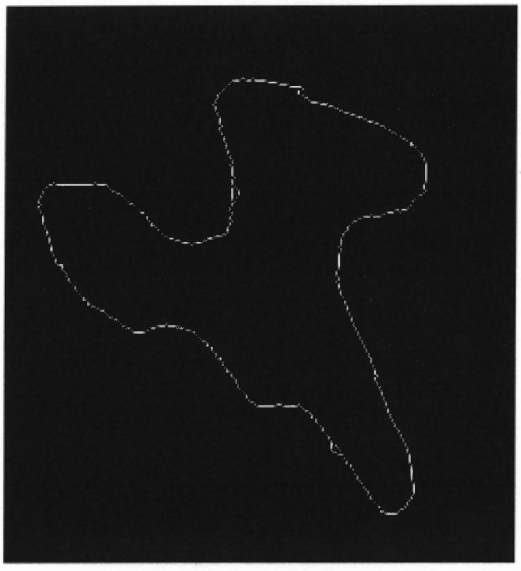

(a)

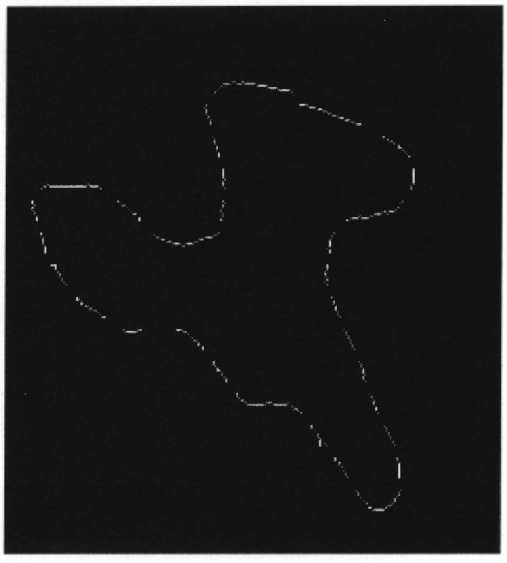

(b)

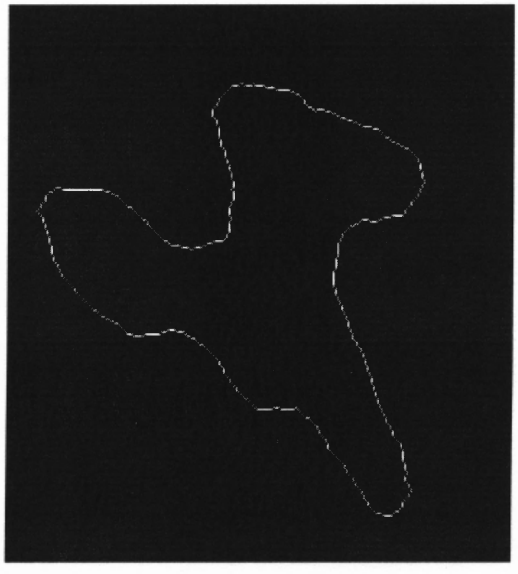

(c)

Figure 3.10 (a) The edge of an industrial part, (b) Its randomly discontinuous edge, and (c) Using the sweep morphological edge-linking algorithm.

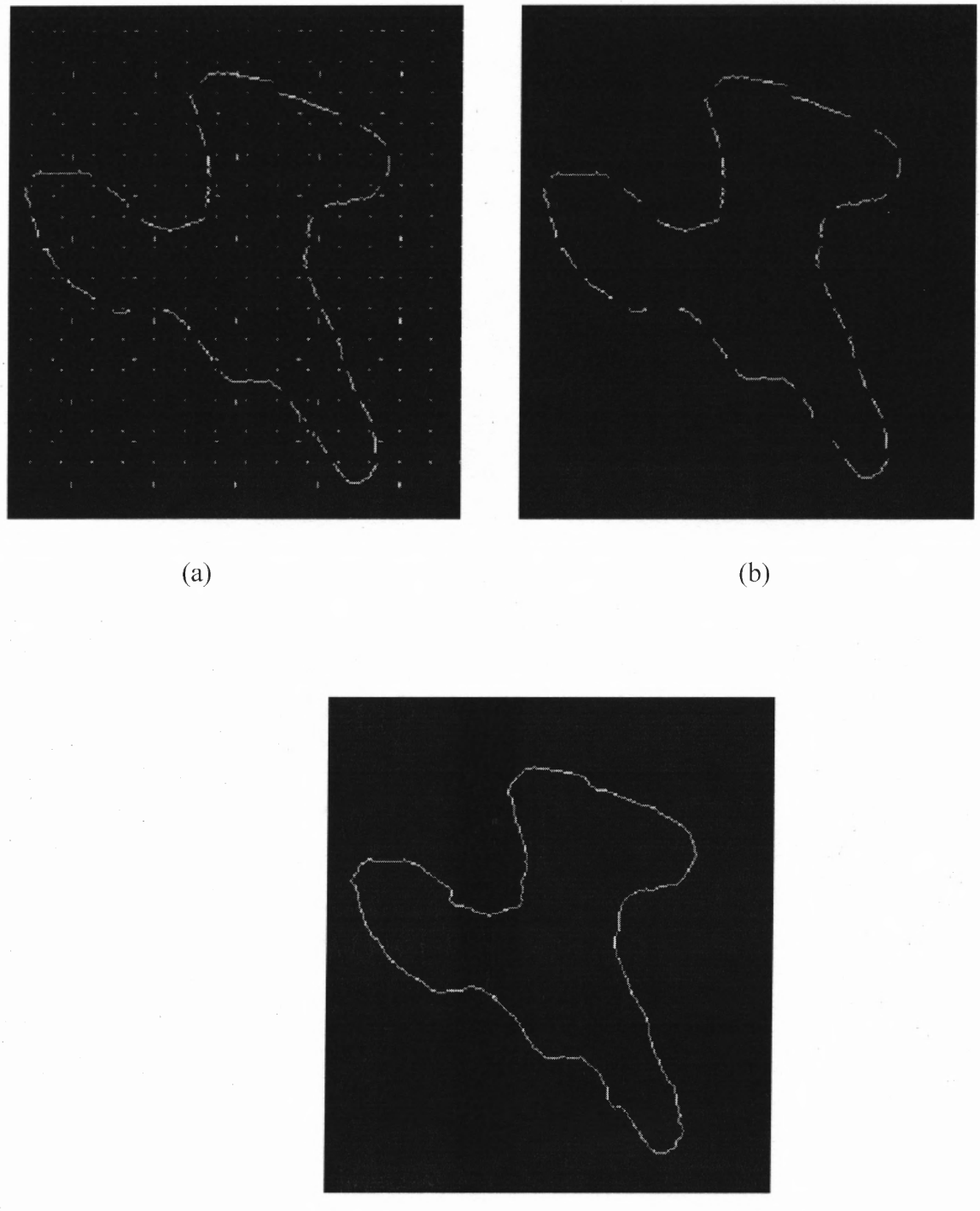

(a) (b)

(c)

Figure 3.11 (a) Part edge with added uniform noise, (b) Part edge after removing noise, and (c) Using the sweep morphological edge-linking algorithm.

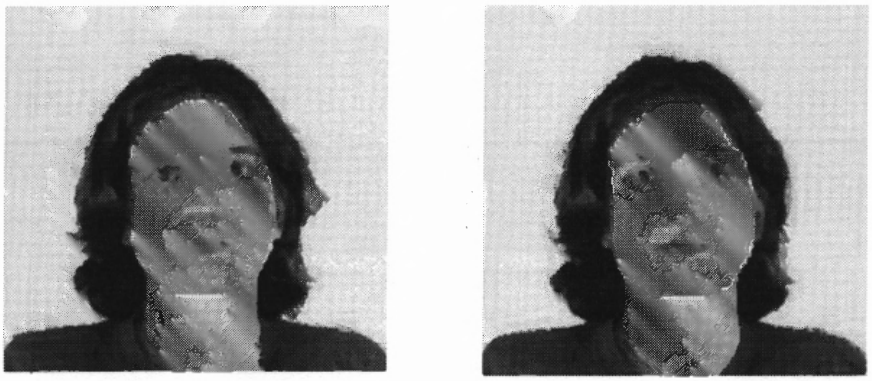

(a) (b)

Figure 3.12 (a) Face image with the originally detected broken edge and (b) Face image with the edge linked by the sweep morphological edge-linking algorithm.

Figure 3.12(a) shows a face image with the originally detected broken edge. Figure 3.12(b) shows the face image with the edge linked by the sweep morphological edge-linking algorithm.

3.6 Shortest Path Planning for Mobile Robot

The recent advances in the fields of robotics and artificial intelligence have stimulated considerable interest in the robot motion planning and the shortest path finding problem [30]. The path planning is in general concerned with finding paths connecting different locations in an environment (e.g., a network, a graph, or a geometric space). Depending on the specific applications, the desired paths often need to satisfy some constraints (e.g., obstacle-avoiding) and optimize certain criteria (e.g., variant distance metrics and cost functions). The problems of planning shortest paths arise in many disciplines, and in fact are one of the several most powerful tools for modeling combinatorial optimization problems.

The path planning problem is given as a mobile robot of arbitrary shape moves from a starting position to a destination in a finite space with arbitrarily shaped obstacles in it. When the traditional mathematical morphology is applied to solve the problem, its drawback is the fixed directional movement of the structuring element (i.e., robot), and is no longer the optimal path in real world applications [34]. By incorporating rotation into the motion of a moving object, it gives more realistic results to solving the shortest path finding problem.

The shortest path-finding problem is equivalent to applying sweep (rotational) morphological erosion to the free space followed by a distance transformation on the domain with the grown obstacles excluded and then tracing back the distance map from the destination point to the neighbors with the minimum distance until the starting point is reached [46]. An example illustrating the shortest path of an H-shaped car by using the sweep (rotational) morphology is shown in Figure 3.13.

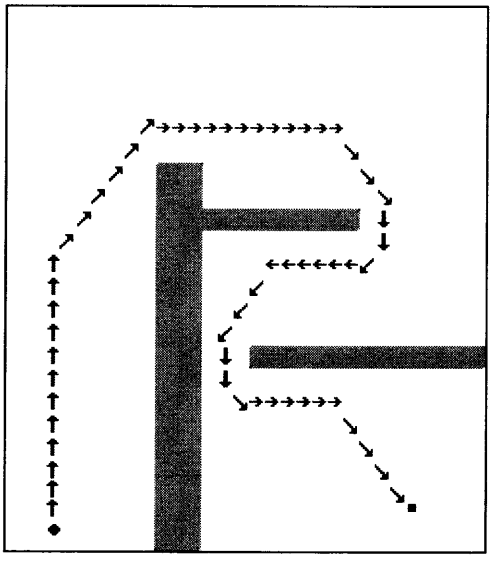

Figure 3.13 Shortest path of an H-shaped car by using the sweep (rotational) morphology.

3.7 Conclusions

This chapter describes the limitation of traditional morphological operations and defines new morphological operations, general sweep morphology. It is shown that traditional morphology is a subset of general sweep morphology. The properties of the sweep morphological operations are studied. The chapter contains several examples of the proposed approach that demonstrate the advantages obtained by using the sweep morphological operations instead of traditional morphological operations.

CHAPTER 4

GEOMETRIC MODELING AND REPRESENTATION

4.1 Introduction

The geometric modeling is the foundation for CAD/CAM integration. The goal for the automated manufacturing inspection and robotic assembly is to generate a complete process automatically. The representation must not only possess the nominal geometric shapes, but also reason the geometric inaccuracies (or tolerances) into the locations and shapes of solid objects.

Boundary representation and *Constructed Solid Geometry (CSG) representation* are popularly used as the internal database [55][60] for geometric modeling. Boundary representation consists of two kinds of information – topological information and geometric information – which represent the vertex coordinates, surface equations, and the connectivity among faces, edges, and vertices. There are several advantages in boundary representation: large domain, unambiguity, uniqueness, and explicit representation of faces, edges, and vertices. There are also several disadvantages: verbose data structure, difficulty in creating, difficulty in checking validity, and variational information unavailability.

The CSG representation is to construct a complex part by hierarchically combining simple primitives using Boolean set operations [43]. There are several advantages in the CSG representation: large domain, unambiguity, easy-to-check validity, and easy creativity. There are also several disadvantages: non-uniqueness, difficulty in editing graphically, input data redundancy, and variational information unavailability.

The framework proposed for geometric modeling and representation is *sweep mathematical morphology* presented in chapter 3, which is based on set-theoretic concept along with geometric sweep. The *sweep* operation to generate a volume by sweeping a primitive object along a space curve trajectory provides a natural design tool. The simplest sweep is *linear extrusion* defined by a 2-D area swept along a linear path normal to the plane of the area to create a volume [54]. Another sweep is *rotational sweep* defined by rotating a 2-D object about an axis.

A generalized sweeping method for CSG modeling was developed by Shiroma *et al.* [74] to generate a swept volume. It is shown that the complex solid shapes can be generated with a blending surface to join two disconnected solids, fillet volumes for rounding corners, and swept volumes formed by the movement of NC (Numeric Control) tools. Ragothama and Shapiro [52] presented a B-Rep method for deformation in parametric solid modeling.

In this chapter, the author presents a method of geometric modeling and representation based on sweep mathematical morphology. It is organized as follows. Section 2 describes modeling based on the sweep mathematical morphology. Section 3 describes the formal languages. Section 4 proposes the representation scheme for two-dimensional and three-dimensional objects. Section 5 introduces the adopted grammars. Section 6 applies the parsing algorithm to determine whether a given object belongs to the language. Conclusions are made in Section 7.

4.2 Geometric Modeling and Sweep Mathematical Morphology

Schemes based on sweep representation are useful in creating solid models of two-and-a-half-dimensional objects that include both solids of uniform thickness in a given direction and axis-symmetric solids. Computer representation of the swept volume of a planar surface has been used as a primary modeling scheme in solid modeling systems [4][75]. Representation of the swept volume of a three-dimensional object [47][82][83], however, has received limited attention.

Leu, Park and Wang [33] presented a method for representing the swept volumes of translating objects using boundary representation and ray in-out classification. Their method is restricted to translation only. Representing the swept volumes of moving objects under a general motion is a more complex problem. A number of researchers have examined the problem of computing swept volumes, including Korein [27] for rotating polyhedra, Kaul [25] using Minkowski sums for translation, Wang and Wang [83] using envelop theory, and Martin and Stephenson [38] using envelop theory and computer algebraic techniques.

Geometric modeling based on sweep morphology is proposed. Because of morphological operators' geometric nature and non-linear property, some modeling problems will become simple and intuitive. This framework can be used for modeling not only swept surface and volumes but also for tolerance modeling in manufacturing.

4.2.1 Tolerancing Expression

Tolerances constrain an object's features to lie within regions of space called *tolerance zones*. Tolerance zones in Rossignac and Requicha [56][61] were constructed by expanding the nominal feature to obtain the region bounded by the outer closed curve,

shrinking the nominal feature to obtain the region bounded by the inner curve, and then subtracting the two resulting regions. This procedure is equivalent to the morphological dilation of the offset inner contour with a tolerance-radius disked structuring element. Figure 4.1(a) shows an annular tolerance zone that corresponds to a circular hole, and Figure 4.1(b) shows a tolerance zone for an elongated slot. Both can be constructed by dilating the nominal contour with a tolerance-radius disked structuring element as shown in Figure 4.2. The tolerance zone for testing the size of a round hole is an annular region lying between two circles with the specified maximal and minimal diameters; the zone corresponding to a form constraint for the hole is also an annulus, defined by two concentric circles whose diameters must differ by a specified amount but are otherwise arbitrary.

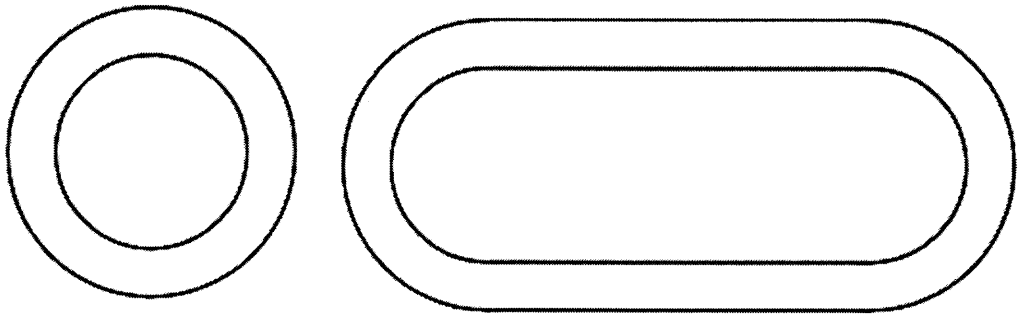

(a) (b)

Figure 4.1 Tolerance zones. (a) An annular tolerance zone that corresponds to a circular hole. (b) A tolerance zone for an elongated slot.

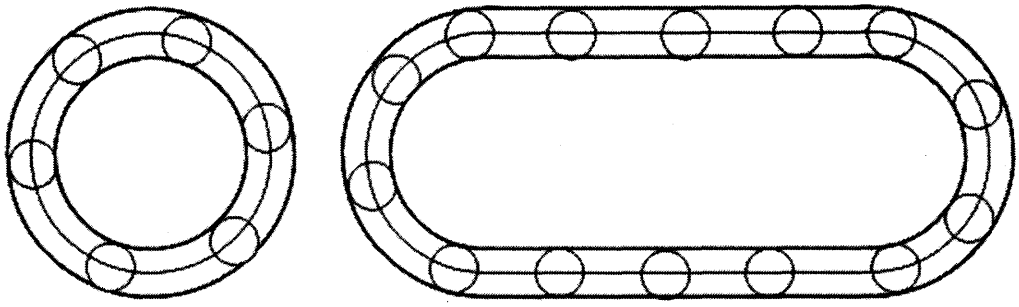

(a) (b)

Figure 4.2 An example of adding tolerance by a morphological dilation.

The sweep mathematical morphology supports the conventional limit (±) tolerance on "dimensions" that appear in the engineering drawings. The positive deviation is equivalent to the dilated result and the negative deviation is equivalent to the eroded result. The industrial parts adding tolerance information can be expressed using a dilation with a circle.

4.2.2 Sweep Surface Modeling

Simplest sweep surface is generated by a profile sweeping along a spine with or without deformation. This is nothing but sweep mathematical dilation of the two curves. Let $P(u)$ be the profile curve, $B(w)$ be the spine, and $S(u,w)$ be the sweep surface. The sweep surface can be expressed as

$$S(u,w) = P(u) \boxplus B(w).$$

A sweep surface with initial and final profiles $P_1(u)$ and $P_2(u)$ at relative locations O_1 and O_2 respectively and with the sweeping rule $R(w)$ is shown in Figure 4.3 and can be expressed as

$$S(u,w) = \{[1\text{-}R(w)][P_1(u) \boxplus (B(w) - O_1)]\} + \{R(w)[P_2(u) \boxplus (B(w) - O_2)]\}.$$

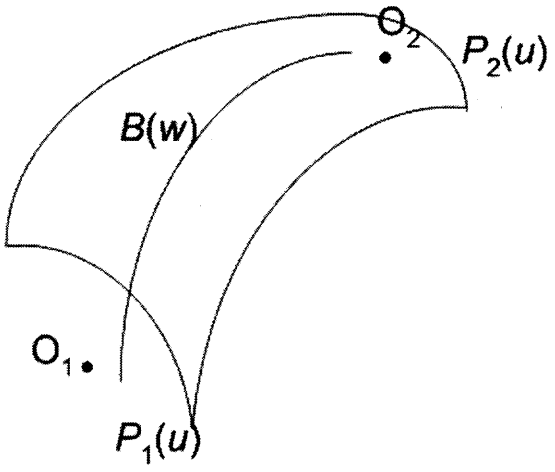

Figure 4.3 Modeling of sweep surface.

4.3 Formal Languages and Sweep Mathematical Morphology

The proposed representation framework is formulated as follows. Let E^N denote the set of points in the N-dimensional Euclidean space and $p = (x_1, x_2, \ldots, x_N)$ represent a point in E^N. In this way, any object is a subset in E^N. The formal model for geometric modeling is a context-free grammar, G, consisting of a four-tuple [17][18][72]:

$G = (V_N, V_T, P, S)$,

where V_N is a set of nonterminal symbols, such as complicated shapes; V_T is a set of terminal symbols that contain two sets: one is the decomposed primitive shapes, such as lines and circles, and the other is the shape operators; P is a finite set of rewriting rules or productions denoted by $A \rightarrow \beta$, where $A \in V_N$ and β is a string over $V_N \cup V_T$; S is the start symbol which represents the solid object. The operators used include sweep morphological dilation, set union, and set subtraction. Note that such a production allows the nonterminal A to be replaced by the string β independent of the context in which A appears.

The grammar G is context-free, since in each production the left part is a single nonterminal and the right part is a nonempty string of terminals and nonterminals. The languages generated by the context free grammars are called context-free languages. Object representation can be viewed as a task of converting a solid shape into a sentence in the language, whereas object classification is the task of "parsing" a sentence.

The criteria for the primitive selection are influenced by the nature of data, the specific application in question, and the technology available for implementing the system. The following serves as a general guideline for the primitive selection.

(1) The primitives should be the basic shape elements that can provide a compact but adequate description of the object shape in terms of the specified structural relations (e.g., the concatenation relation).

(2) The primitives should be easily extractable by the existing nonsyntactic (e.g., decision-theoretic) methods, since they are considered to be simple and compact shapes and their structural information is not important.

4.4 Representation Scheme

4.4.1 Two-dimensional Attributes

Commonly used two-dimensional attributes are rectangle, parallelogram, triangle, rhombus, circle, and trapezoid. They can be represented easily by using the sweep morphological operators. The expressions are not unique, and the preference depends on the simplest combination and the least computational complexity. The common method is to decompose the attributes into smaller components and apply morphological dilations to grow these components. Let $\boldsymbol{a}$ and $\boldsymbol{b}$ represent unit vectors in x- and y-axes,

respectively. Note that when the sweep dilation is not associated with rotation and scaling, it is equivalent to the traditional dilation.

(a) *Rectangle*: It is represented as a unit x-axis vector $\boldsymbol{a}$ swept along a unit y-axis vector $\boldsymbol{b}$, i.e., $\boldsymbol{b} \boxplus \boldsymbol{a}$ with no rotation or scaling.

(b) *Parallelogram*: Let $\boldsymbol{k}$ denote a vector sum of $\boldsymbol{a}$ and $\boldsymbol{b}$ that are defined in (a). It is represented as $\boldsymbol{k} \boxplus \boldsymbol{a}$ with no rotation or scaling.

(c) *Circle*: Using a sweep rotation, a circle can be represented as a unit vector $\boldsymbol{a}$ swept about a point p through 2π degrees, i.e., $p \boxplus \boldsymbol{a}$.

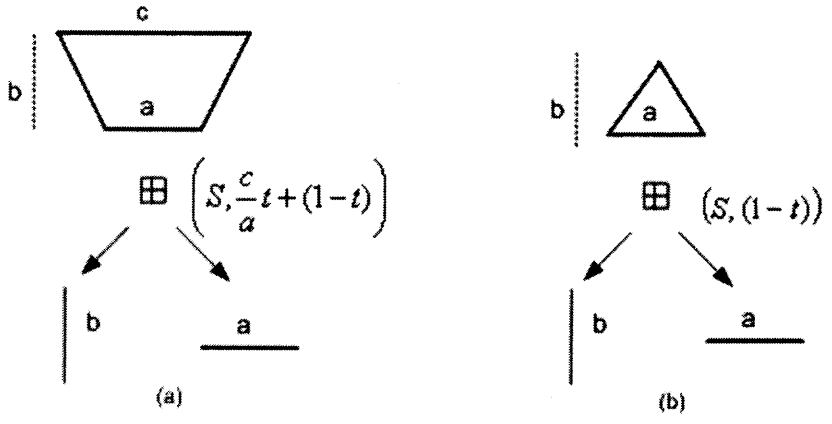

Figure 4.4 The Decomposition of two-dimensional attributes.

(d) *Trapezoid*: $\boldsymbol{b} \boxplus \boldsymbol{a}$ with a linear scaling factor to change a magnitude of $\boldsymbol{a}$ into $\boldsymbol{c}$ as it is swept along $\boldsymbol{b}$ as shown in Figure 4.4(a). Let $0 \le t \le 1$. The scaling factor along the trajectory $\boldsymbol{b}$ is $S(t) = \frac{c}{a}t + (1-t)$.

(e) *Triangle*: $\boldsymbol{b} \boxplus \boldsymbol{a}$, similar to trapezoid but with a linear scaling factor to change a magnitude of $\boldsymbol{a}$ into zero as it is swept along $\boldsymbol{b}$, as shown in Figure 4.4(b).

4.4.2 Three-dimensional Attributes

The three-dimensional attributes can be applied by the similar method. Let ***a***, ***b***, ***c*** denote unit vectors in *x*-, *y*-, and *z*-axes, respectively. The formal expressions are presented below.

(a) *Parallelepiped*: It is represented as a unit vector ***a*** swept along a unit vector ***b*** to obtain a rectangle and then it is swept along a unit vector ***c*** to obtain the parallelepiped, i.e., ***c*** ⊞ (***b*** ⊞ ***a***).

(b) *Cylinder*: It is represented as a unit vector ***a*** swept about a point *p* through 2π degrees to obtain a circle, and then it is swept along a unit vector ***c*** to obtain the cylinder, i.e., ***c*** ⊞ (*p* ⊞ ***a***).

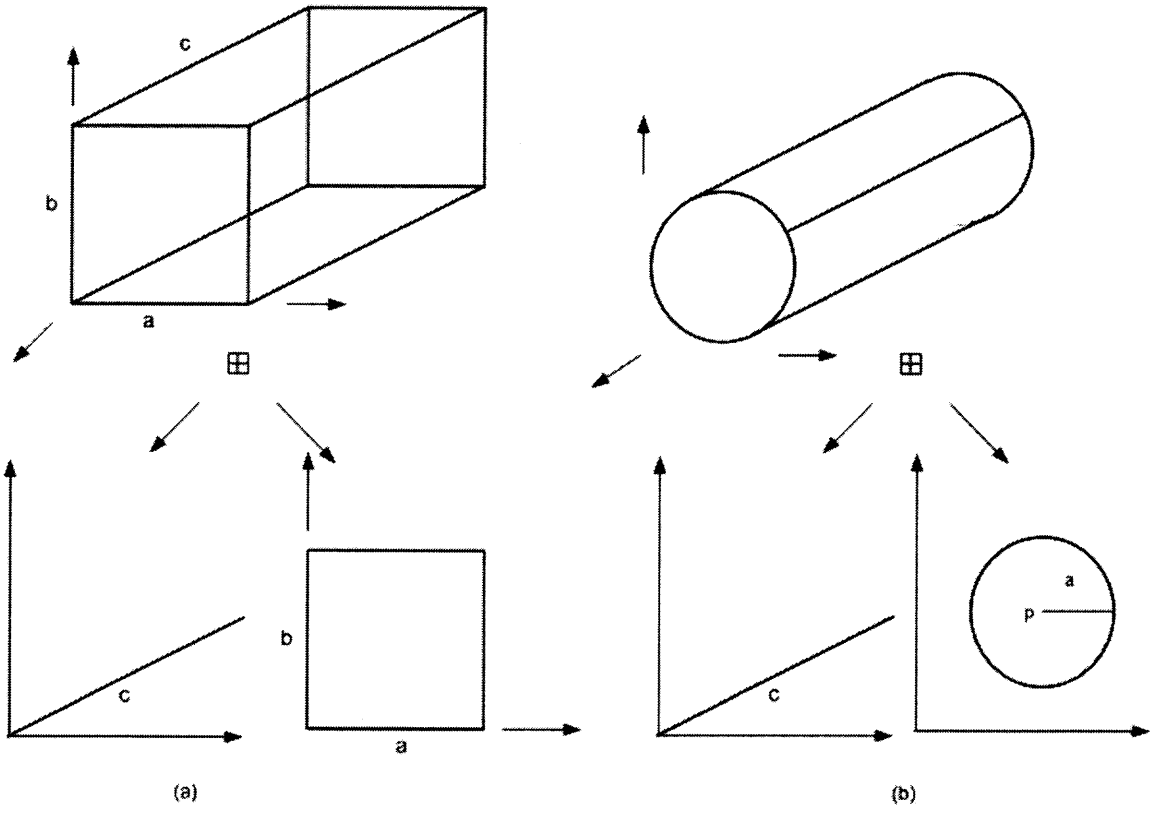

Figure 4.5 The Decomposition of three-dimensional attributes.

(c) *Parallelepiped with corner truncated by a sphere*: A unit vector $\boldsymbol{a}$ is swept along a unit vector $\boldsymbol{b}$ to obtain a rectangle. A vector $\boldsymbol{r}$ is swept about a point p through 2π degrees to obtain a circle, and then it is subtracted from the rectangle. The result is swept along a unit vector $\boldsymbol{c}$, i.e., $\boldsymbol{c} \boxplus [(\boldsymbol{b} \boxplus \boldsymbol{a}) - (p \boxplus \boldsymbol{r})]$, as shown in Figure 4.6.

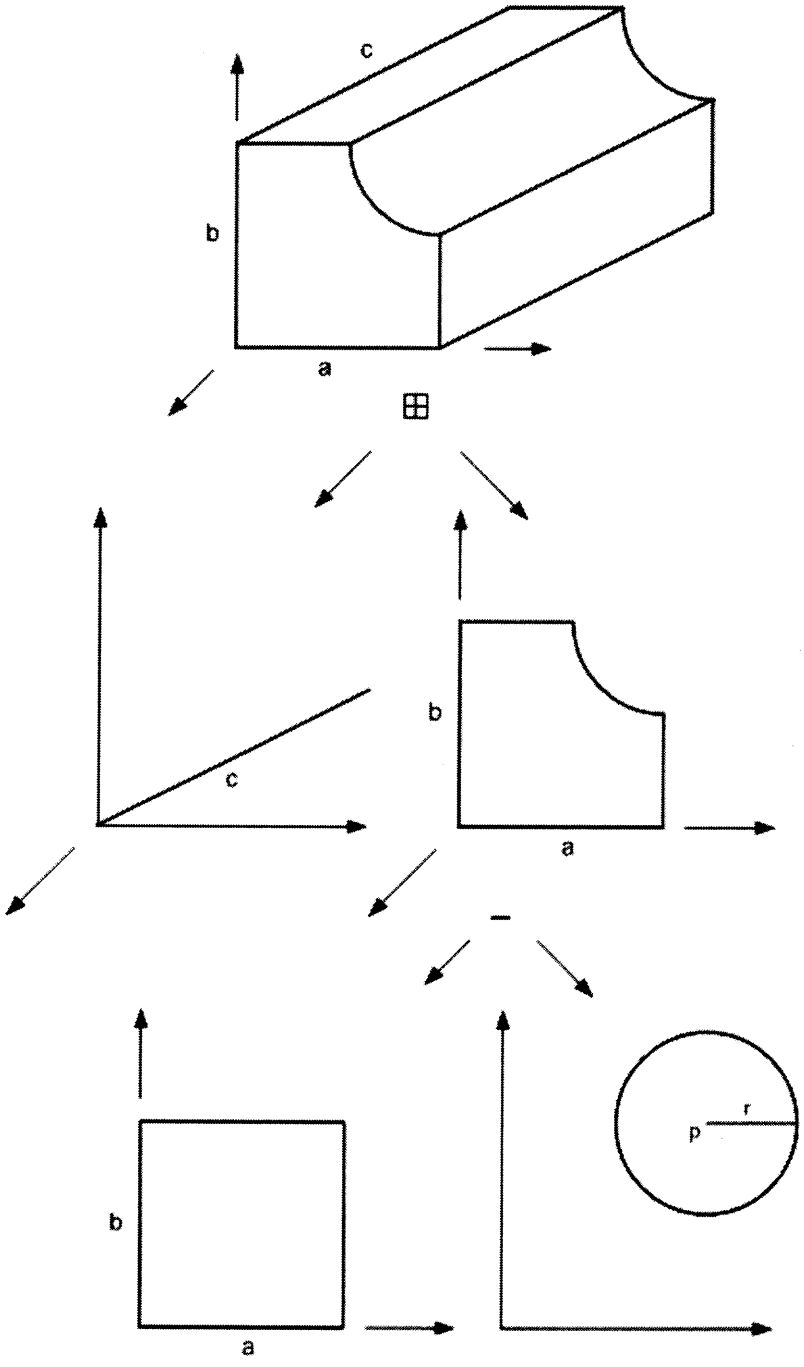

Figure 4.6 Sweep dilation of a rectangle with a corner truncated by a circle.

(d) *Sweep dilation of a square along a trajectory with deformation to a circle*: The square is represented as a rational B-spline curve. The polygon net is specified by a square with 9 points with the first and the last being the same and the weights of the corner vary from 5 to $\sqrt{2}/2$ as it is swept along the trajectory $\boldsymbol{C}$ that is defined in the parametric form as $x = 10s$ and $y = \cos(\pi s) - 1$. The sweep transformation is given by

$$[Sw_T] = \begin{bmatrix} \cos\psi & \sin\psi & 0 & 0 \\ -\sin\psi & \cos\psi & 0 & 0 \\ 0 & 0 & 1 & 0 \\ 10s & \cos\pi s & 0 & 1 \end{bmatrix}, \text{ where } \psi = \tan^{-1}\left(\frac{-\pi \sin(\pi s)}{10}\right).$$

The formal expression is $\boldsymbol{C} \boxplus \boldsymbol{B}$. The sweeping of a square along a trajectory with deformation to a circle is shown in Figure 4.7.

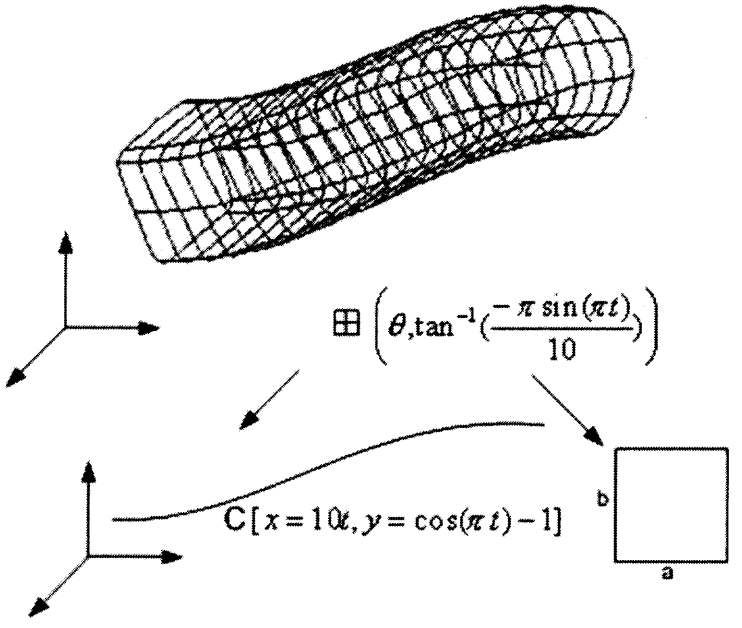

Figure 4.7 Sweeping of a square along a trajectory with deformation to a circle.

(e) *Parallelepiped with a cylindrical hole*: A unit vector $\boldsymbol{a}$ is swept along a unit vector $\boldsymbol{b}$ to obtain a rectangle. A vector $\boldsymbol{r}$ is swept about a point p through 2π degrees to obtain a circle, and it is subtracted from the rectangle. The result is swept along a unit vector $\boldsymbol{c}$, i.e., $\boldsymbol{c} \boxplus [(\boldsymbol{b} \boxplus \boldsymbol{a}) - (p \boxplus \boldsymbol{r})]$, as shown in Figure 4.8.

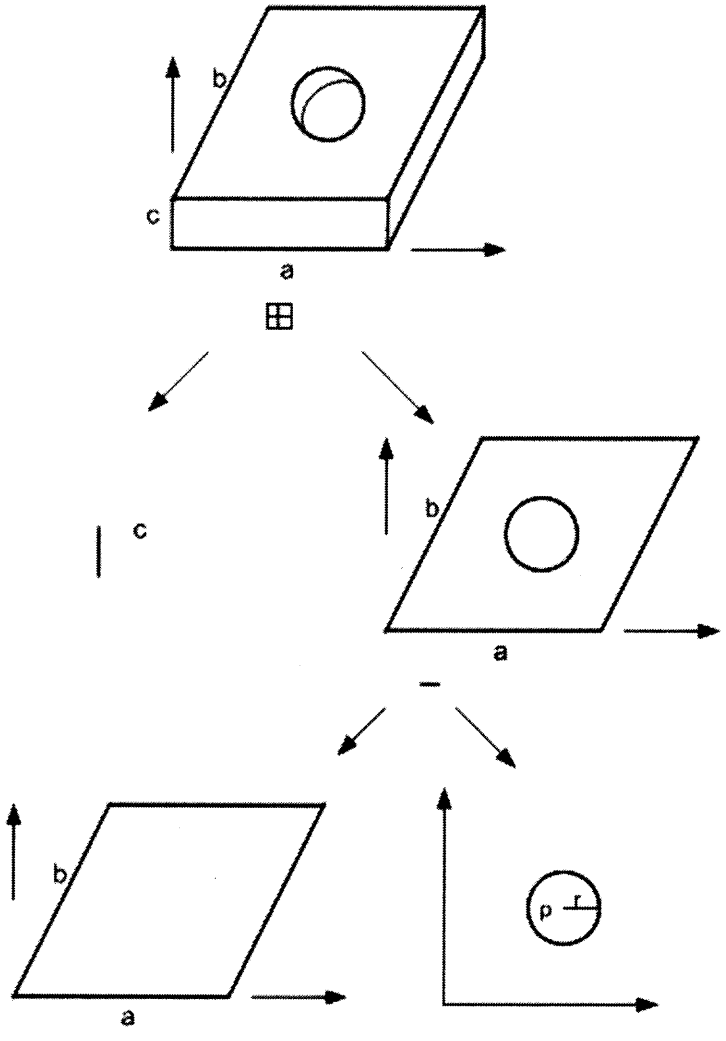

Figure 4.8 Sweep dilation of a rectangle with a circular hole.

(f) *U-shape block*: A unit vector $\boldsymbol{a}$ is swept along a unit vector $\boldsymbol{b}$ to obtain a rectangle. A vector $\boldsymbol{r}$ is swept about a point p through π degrees to obtain a half circle, and it is dilated along the rectangle to obtain a two-rounded-corner rectangle that is then subtracted from

another rectangle to obtain a U-shaped two-dimensional object. The result is swept along a unit vector $\boldsymbol{c}$ to obtain the final U-shaped object, i.e., $\boldsymbol{c} \boxplus [(\boldsymbol{b}' \boxplus \boldsymbol{a}') - [(\boldsymbol{b} \boxplus \boldsymbol{a}) \boxplus (p \boxplus \boldsymbol{r})]]$, as shown in Figure 4.9.

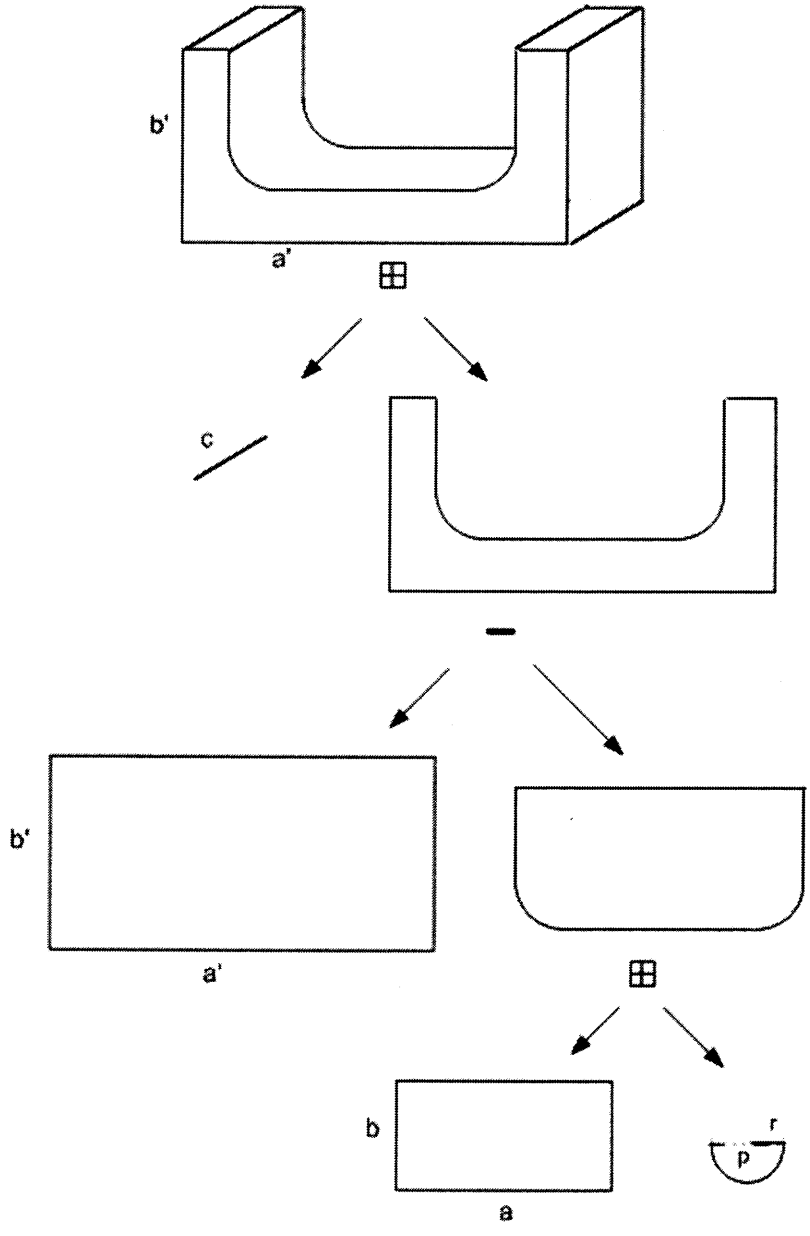

Figure 4.9 Machining with a round bottom tool.

Note that the proposed sweep mathematical morphology model can be applied to the NC machining process. For example, the ball-end milling cutter can be viewed as the structuring element and it can be moved along a predefined path to cut a work piece. During the movement, the cutter can be rotated to be perpendicular to the sweep path. If the swept volume is subtracted from the work piece, the remaining part can be obtained.

4.5 Grammars

4.5.1 Two-dimensional Attributes

All the primitive two-dimensional objects can be represented by the following grammar using the sweep mathematical morphology model:

$$G = (V_N, V_T, P, S),$$

where,

$$V_N = \{S, A, B, K\}, V_T = \{ a, b, k, p, \boxplus\},$$

P: $S \rightarrow B \boxplus A \mid B \boxplus K \mid p \boxplus A,$

$A \rightarrow aA \mid a,$

$B \rightarrow bB \mid b,$

$K \rightarrow kK \mid k.$

The sweep dilation $\boxplus$ can be $\oplus$ ($S = 0$, $\theta = 0$), $\oplus$ ($S = \frac{c}{a}t + (1-t)$, $\theta = 0$), or $\oplus$ ($S = 0$, $\theta = 2\pi$).

(a) *Rectangle* can be represented by the string $bb\boxplus aa$, with a's and b's repeated any number of times depending on the required size.

(b) *Parallelogram* can be represented by the string $kk\boxplus aaa$, with a's and k's repeated any number of times depending on the required size.

(c) *Circle* can be represented by the string $p\boxplus aaa$, with a's repeated any number of times depending on the required size and with $\boxplus$ as $\oplus$ ($S = 0$, $\theta = 2\pi$).

(d) *Trapezoid* can be represented by the string $bb\boxplus aa$, with a's and b's repeated any number of times depending on the required size and with $\boxplus$ as $\oplus$ ($S = \frac{c}{a}t + (1-t)$, $\theta = 0$).

(e) *Triangle* can be represented by the string $bb\boxplus aa$, with a's and b's repeated any number of times depending on the required size and with $\boxplus$ as $\oplus$ ($S = (1-t)$, $\theta = 0$).

4.5.2 Three-dimensional Attributes

All the primitive three-dimensional objects can be categorized into the following grammar:

$$G = (V_N, V_T, P, S),$$

where

$$V_N = \{S, A, B, C\}, V_T = \{ a, b, c, p, (,), \boxplus\},$$

P: $S \rightarrow C \boxplus (B \boxplus A) \mid C \boxplus (p \boxplus A)$,

$A \rightarrow aA \mid a$,

$B \rightarrow bB \mid b$,

$C \rightarrow cC \mid c$.

The sweep dilation ⊞ can be either ⊕ ($S = 0$, $\theta = 0$) or ⊕ ($S = 0$, $\theta = 2\pi$).

(a) *Parallelepiped* can be represented by the string *ccc*⊞(*bb*⊞*aaa*), with *a*'s, *b*'s, and *c*'s repeated any number of times depending on the required size.

(b) *Cylinder* can be represented by the string *cccc*⊞(*p*⊞*aaa*), with *a*'s and *c*'s repeated any number of times depending on the required size and with the first dilation operator ⊞ as ⊕ ($S = 0$, $\theta = 2\pi$) and the second dilation as the traditional dilation.

(c) Consider the grammar

$$G = (V_N, V_T, P, S),$$

where,

$$V_N = \{A, B, C, N\},\ V_T = \{ a, b, c, p, \boxplus, -, (,)\},$$

P: $S \rightarrow C \boxplus N$,

$N \rightarrow$ rectangle – circle,

$C \rightarrow cC \mid c$

The productions for the rectangle and circle are given in Section 4.6.1.

(c.1) The *sweep dilation of a rectangle with a corner truncated by a circle* can be represented by the string *cc*⊞((*bb*⊞*aaa*)−(*p*⊞*aa*)), with *a*'s, *b*'s, and *c*'s repeated any number of times depending on the required size and with the second dilation operator ⊞ as ⊕ ($S = 0$, $\theta = 2\pi$).

(c.2) The *sweep dilation of a rectangle with a circular hole* can be represented by the string $cc\boxplus((bb\boxplus aaa)-(p\boxplus a))$, with a's, b's, and c's repeated any number of times depending on the required size and with the second dilation operator $\boxplus$ as $\oplus$ ($S = 0$, $\theta = 2\pi$). The difference from the previous one is that the circle lies completely within the rectangle, and hence a hole is obtained instead of a truncated corner.

(d) The grammar for the U-shape block can be represented as follows:

$$G = (V_N, V_T, P, S),$$

where

$$V_N = \{A, B, C, N, M, \text{half\_circle}\},\ V_T = \{a, b, c, p, \boxplus, -\},$$

P: $S \rightarrow C \boxplus N,$

$N \rightarrow$ rectangle $- M,$

$C \rightarrow cC \mid c,$

$M \rightarrow$ rectangle $\boxplus$ half_circle,

half_circle $\rightarrow p \boxplus A.$

The *U-shape block* can be represented by the string $ccc\boxplus(bbb\boxplus aaaa-((bb\boxplus aa)\boxplus(p\boxplus a)))$, with a's, b's, and c's repeated any number of times depending on the required size and with the fourth dilation operator $\boxplus$ as $\oplus$ ($S = 0$, $\theta = \pi$).

4.6 Parsing Algorithm

Given a grammar G and an object representation as a string, the string can be parsed to find out whether it belongs to the given grammar. There are various parsing algorithms, among which Earley's parsing algorithm for context-free grammars is very popular. Let V^* denote the set of all sentences composed of elements from V. The algorithm is described as follows:

Input: Context-free Grammar $G = (V_N, V_T, P, S)$ and an input string $w = a_1a_2...a_n$ in V_T^*.

Output: The parse lists $I_0, I_1, ..., I_n$.

Method: First construct I_0 as follows:

1. If $S \rightarrow \alpha$ is a production in P, add $[S \rightarrow .\alpha, 0]$ to I_0.

Now, perform steps 2 and 3 until no new item can be added to I_0.

2. If $[B \rightarrow \gamma., 0]$ is on I_0, add $[A \rightarrow \alpha B.\beta, 0]$ for all $[A \rightarrow \alpha.B\beta, 0]$ on I_0.

3. Suppose that $[A \rightarrow \alpha.B\beta, 0]$ is an item in I_0. Add to I_0 for all productions in P of the form $B \rightarrow \gamma$, the item $[B \rightarrow .\gamma, 0]$ (provided this item is not already in I_0).

Now, construct I_j by having constructed $I_0, I_1, ..., I_{j-1}$.

4. For each $[B \rightarrow \alpha.a\beta, i]$ in I_{j-1} such that $a = a_j$, add $[B \rightarrow \alpha a.\beta, i]$ to I_j.

Now, perform steps 5 and 6 until no new items can be added.

5. Let $[A \rightarrow \gamma., i]$ be an item in I_j. Examine I_i for items of the form $[B \rightarrow \alpha.A\beta, k]$. For each one found, add $[B \rightarrow \alpha A.\beta, k]$ to I_j.

6. Let $[A \rightarrow \alpha.B\beta, i]$ be an item in I_j. For all $B \rightarrow \gamma$ in P, add $[B \rightarrow .\gamma, j]$ to I_j.

The algorithm, then, is to construct I_j for $0 < j \leq n$. Some examples of the parser are shown below.

Example 1. Rectangle represented by the string b⊞aa and the given grammar is

$$G = (V_N, V_T, P, S),$$

where

$$V_N = \{S, A, B\}, V_T = \{a, b, \boxplus\},$$

P: $S \rightarrow B \boxplus A,$

$A \rightarrow aA \mid a,$

$B \rightarrow bB \mid b.$

The parsing lists obtained are as follows:

I_0	I_1	I_2	I_3	I_4
$[S\rightarrow .B\boxplus A, 0]$	$[B\rightarrow b.B, 0]$	$[S\rightarrow B\boxplus .A, 0]$	$[A\rightarrow a.A, 2]$	$[A\rightarrow a.A, 3]$
$[B\rightarrow .bB, 0]$	$[B\rightarrow b., 0]$	$[A\rightarrow .aA, 2]$	$[A\rightarrow a., 2]$	$[A\rightarrow a., 3]$
$[B\rightarrow .b, 0]$	$[S\rightarrow B.\boxplus A, 0]$	$[A\rightarrow .a, 2]$	$[S\rightarrow B\boxplus A., 0]$	$[A\rightarrow aA., 2]$
	$[B\rightarrow .bB, 1]$		$[A\rightarrow .aA, 3]$	$[A\rightarrow .aA, 4]$
	$[B\rightarrow .b, 1]$		$[A\rightarrow .a, 3]$	$[A\rightarrow .a, 4]$
				$[S\rightarrow B\boxplus A., 0]$

Since $[S\rightarrow A\boxplus B., 0]$ is in the last list, the input belongs to the language $L(G)$ generated by G.

Example 2. Consider the string $b \boxplus ba$ and the given grammar is

$$G = (V_N, V_T, P, S),$$

where

$$V_N = \{S, A, B\}, V_T = \{ a, b, \boxplus\},$$

P: $S \rightarrow B \boxplus A,$

$A \rightarrow aA \mid a,$

$B \rightarrow bB \mid b.$

The parsing lists are as follows:

I_0	I_1	I_2	I_3
$[S\rightarrow .B\boxplus A, 0]$	$[B\rightarrow b.B, 0]$	$[S\rightarrow B\boxplus .A, 0]$	*Nil*
$[B\rightarrow .bB, 0]$	$[B\rightarrow b., 0]$	$[A\rightarrow .aA, 2]$	
$[B\rightarrow .b, 0]$	$[S\rightarrow B.\boxplus A, 0]$	$[A\rightarrow .a, 2]$	
	$[B\rightarrow .bB, 1]$		
	$[B\rightarrow .b, 1]$		

Since there is no production starting with S in the last list, the input does not belong to the language generated by G.

Considering a rectangle and trapezoid the string representation is $bb \boxplus aa$, same for both but the difference is in the dilation operator representation. Rectangle is represented by the dilation with no scaling and rotation whereas trapezoid has a dilation $\boxplus$ as $\oplus$ ($S = (1-t)$, $\theta = 0$). Both will be classified into the same broader group of quadrilaterals but into different subgroups.

Consider the swept surface shown in Figure 4.10. Its string representation is the same as the swept surface shown in Figure 4.7. The only difference is that it is not deformed as being swept.

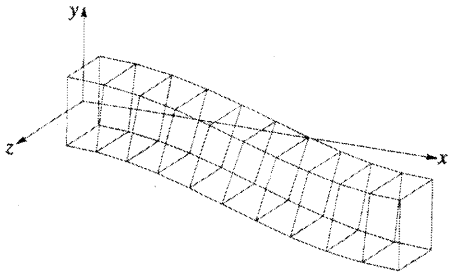

Figure 4.10 An example of swept surface.

4.7 Conclusions

This chapter presented a method of geometric modeling and representation based on sweep mathematical morphology. Since the shape and the dimension of a 2-D structuring element can be varied during the process, not only simple rotational and extruded solids but also more complicated objects with blending surfaces can be generated by sweep morphology. The author has developed grammars for solid objects and has applied Earley's parser algorithm to determine whether a given string belongs to a group of similar objects. It is demonstrated that the sweep mathematical morphology is an efficient tool for geometric modeling and representation in an intuitive manner.

CHAPTER 5

SUMMARY AND FUTURE RESEARCH

This dissertation is aimed to investigate image processing techniques especially in the implementation of mathematical morphology and to develop new morphological operators, which can be applied to image analysis and object representation. This final chapter summarizes the contributions of this research and briefly discuss the further potential research.

The limitations of traditional morphological operations are discussed and a new class of morphological operations, general sweep morphology, is defined. It is shown that traditional morphology is a subset of general sweep morphology. The properties of the sweep morphological dilation and erosion are studied. It is shown that sweep morphological operations possess many properties of traditional morphological operations.

The sweep mathematical morphology can be used to generate 3-D objects. Since the shape and the dimension of a 2-D structuring element can be varied during the process, not only simple rotational and extruded solids but also more complicated objects with blending surfaces can be generated. Shih and Gaddipati [67] demonstrated the blending of swept surfaces with deformations using the general sweep morphological operation. Potential future research could be in studying the relations between these operations and order-statistic filters and fuzzy morphology. Also investigate other applications areas where this new class of operations can be used.

Compared to traditional morphological operations, sweep morphological operations are computationally expensive because of the rotation and scaling factors. As traditional mathematical morphology is a subset of sweep mathematical morphology, some properties of traditional mathematical morphology are satisfied only under conditional constraints. In spite of these limitations, it is demonstrated that sweep mathematical morphology has various useful applications.

The sweep morphological opening can be used for image enhancement. It has been shown that sweep morphological opening preserves object features while removing the noise better than traditional opening, where object features smaller than the structuring element are also lost.

Another application of sweep mathematical morphology is for edge linking, where it is shown that sweep morphological dilation with elliptical structuring element does a far better job in edge linking than traditional dilation and thus demonstrating the advantages of the developed approach over traditional morphological operations.

Another application of general sweep mathematical morphology is in the work of motion planning. Modern manufacturing and other high technology fields of robotics and artificial intelligence have simulated considerable interest in motion planning problems. It has been shown that sweep mathematical morphology can be used to solve more realistic motion-planning problems in which the moving object is not restricted to translation motion, but rotational factor is also incorporated into it. Future work is to investigate potentially more efficient method of motion planning which retains more of the object geometry in the construction of optimal paths.

It is shown that regulated morphological operations give better results for corner detection in binary images than Laganiere's method. Also it was shown that there is substantial reduction in computation as this uses one structuring element where as Laganiere method uses four structuring elements.

Application of syntactic pattern recognition to solid modeling using sweep mathematical morphology is discussed. Sweep mathematical morphology is demonstrated as an intuitive and efficient tool for geometric modeling and representation. Grammars are defined for the swept solid objects and their string representation are given. It is shown that given the string representation of an object how it can be classified into a broader group and later into a subgroup studying the sweep dilation properties. Future research will study more complex objects and include grammatical inference for learning the automata from sample patterns. Another challenging research lies in automating the representation of swept objects. This approach can be extended beyond CAD/CAM into biotechnology and other related fields.

The goal in this dissertation was to study mathematical morphology. Existing mathematical morphological operators were studied and weakness of these operators was found and overcome. The final result is that this dissertation has developed new class of mathematical morphology called sweep mathematical morphology and studied their properties. Various applications are also illustrated. The author strongly hopes that this dissertation will be useful in various other applications.

REFERENCES

[1] Agam, G. and Dinstein, I., "Regulated morphological operations," *Pattern Recognition,* vol. 32, pp. 947-971, 1999.

[2] Beaudet, P. R., "Rotationally invariant image operators," *International Joint Conference on Pattern Recognition,* pp. 579-583, 1978.

[3] Bloch, J. and Maitre, H., "Fuzzy mathematical morphology," *Ann. Math. Artificial Intell.,* vol. 10, pp. 55-84, 1994.

[4] Brooks, R. A., "Symbolic reasoning among 3-D models and 2-D images," *Artificial Intelligence*, vol. 17, pp. 285-348, 1981.

[5] Chanda, B., Kundu, M. K., and Padmaja, Y. V., "A Multi-scale morphologic edge detector," *Pattern Recognition,* vol. 31, no. 10, pp. 1469-1478, 1998.

[6] Chen, C., Hung, Y., and Wu, J., "Space-varying mathematical morphology for adaptive smoothing of 3D range data." *Asia Conference on Computer Vision*, Osaka, Japan, pp. 23-25, Nov. 1993.

[7] Chen, C. S., Wu, J. L., and Hung, Y. P., "Theoretical aspects of vertically invariant gray-level morphological operators and their application on adaptive signal and image filtering," *IEEE Trans. Signal Processing*, vol. 47, no. 4, April 1999.

[8] Cooper, D., Elliott, H., Cohen, F., and Symosek, P., "Stochastic boundary estimation and object recognition," *Computer Graphics Image Processing,* vol. 12, pp. 326-356, 1980.

[9] Cooper, J., Venkatesh, S., and Kitchen, L., "Early jump-out corner detectors," *IEEE Trans. Pattern Analysis and Machine Intelligence*, vol. 15, no. 8, pp. 823-828, 1993.

[10] Deriche, R. and Giraudon, G., "Accurate corner detection: An analytical study," *Proc. 3rd Int. Conf. on Computer Vision,* pp. 66-70, 1990.

[11] Dougherty, E. and Giardina, C., *Morphological methods in image and signal processing,* Prentice-Hall, Englewood Cliffs, NJ, 1988.

[12] Dreschler, L. and Nagel, H. H., "Volumetric model and 3D trajectory of a moving car derived from monocular TV frame sequences of a street scene," *Computer Vision, Graphics and Image Processing*, vol. 20, no. 3, pp. 199-228, 1981.

[13] Duda, R. O. and Hart, P.E., *Pattern Classification and Scene Analysis*, Wiley, New York, pp. 339, 1973.

[14] Eichel, P. H., Delp, E. J., Koral, K., and Buda, A. J., "A method for a fully automatic definition of coronary arterial edges from cineangiograms," *IEEE Trans. Medical Imaging*, MI-7, pp. 313-320, 1988.

[15] Farag, Aly A., and Delp, Edward J., "Edge linking by sequential search," *Pattern Recognition*, pp. 611-633, 1995.

[16] Foley, J., VanDam, A., Feiner, S., and Hughes, J., *Computer Graphics: Principles and Practice*, second edition, Addison-Wesley, Reading, MA, 1995.

[17] Fu, K. S., *Syntactic Pattern Recognition and Applications*, Prentice Hall, Englewood Cliffs, NJ, 1982.

[18] Ghosh, P. K., "A mathematical model for shape description using Minkowski operators," *Computer Vision, Graphics and Image Processing*, vol. 44, pp. 239-269, 1988.

[19] Giles, R., "Luckasiewicz logic and fuzzy theory," *Internat. J. Man-Mach. Stud.*, vol. 8, 1976.

[20] Gonzalez R. C., and Woods, R. E., *Digital Image Processing*, Addison-Wesley, 2001.

[21] Haralick, R. M., Sternberg, S. K., and Zhuang, X., "Image analysis using mathematical morphology," *IEEE Trans. on Pattern Analysis and Machine Intelligence*, vol. 9, no. 4, pp. 532-550, July 1987.

[22] Harris, C. G., "Determination of ego-motion from matched points," *Proc. Alvey Vision Conf.* 1987.

[23] Harris, C. G. and Stephens, M., "A combined corner and edge detector," *Proc. 4th Alvey Vision Conf.*, pp. 147-151, 1988.

[24] Jang, B. K. and Chin, R. T., "Analysis of thinning algorithms using mathematical morphology," *IEEE Transactions on Pattern Analysis and Machine Intelligence*, vol. 12, no. 6, pp. 541 –551, June 1990.

[25] Kaul, Anil, *Computing Minkowski Sums*, Ph.D. thesis, Department of Mechanical Engineering, Columbia University, 1993.

[26] Kitchen, L. and Rosenfeld, A., "Gray-level corner detection," *Pattern Recognition Letters*, pp. 95-102, December 1982.

[27] Korein, J., *A Geometric Investigating Reach*, MIT Press, Cambridge, MA, 1985.

[28] Kuosmanen, P. and Astola, J., "Soft morphological filtering," *J. Math. Imaging Vision*, vol. 5, pp. 231-262, 1995.

[29] Laganiere, R., "A morphological operator for corner detection," *Pattern Recognition,* vol. 31, no. 11, pp. 1643-1652, 1998.

[30] Latombe, J., *Robot Motion Planning*, Kluwer Academic Publishers, 1991.

[31] Lee, J., Haralick, R., and Shapiro, L., "Morphological edge detection," *IEEE Trans. Robotics and Automation,* vol. 3, no. 2, pp. 142-150, April 1987.

[32] Lee, Kil-jae and Bien, Zeungnam, "A gray-level corner detector using fuzzy logic," *Pattern Recognition Letters*, vol. 17, pp. 939-950, 1996.

[33] Leu, M. C., Park, S. H., and Wang, K. K., "Geometric representation of translational swept volumes and its applications," *ASME Journal of Engineering for Industry*, vol. 108, pp. 113-119, 1986.

[34] Lin, P. L. and Chang, S., "A shortest path algorithm for nonrotating object among obstacles of arbitrary shapes," *IEEE Trans. Syst., Man, and Cyber.*, vol. 23, no. 3, pp. 825-832, 1993.

[35] Lin, Rey-Sern, Chu, Chyi-Hwa, and Hsueh, Yuang-Cheh, "A modified morphological corner detector," *Pattern Recognition Letters*, vol. 19, no. 3, pp. 279-286, 1998.

[36] Maragos, P. and Ziff, R., "Threshold superimposition in morphological image analysis systems," *IEEE Transactions on Pattern Analysis and Machine Intelligence*, vol. 12, no. 5, pp. 498-504, 1990.

[37] Martelli, A., "An application of heuristic search methods to edge and contour detection," *Communication ACM,* vol. 19, pp. 73-83, 1976.

[38] Martin, R. R. and Stephenson, P. C., "Sweeping of three dimensional objects," *Computer Aided Design*, vol. 22, no. 4, pp. 223-234, May 1990.

[39] Matheron, G., *Random sets and Integral Geometry*, Wiley, New York, 1975.

[40] Mehrotra, R. and Nichani, S., "Corner detection," *Pattern Recognition,* vol. 23, pp. 1223-1233, 1990.

[41] Morales, A. and Acharya, R., "Statistical analysis of morphological openings," *IEEE Trans. Signal Processing*, vol. 41, no. 10, pp. 3052-3056, 1993.

[42] Moravec, H. P., "Towards automatic obstacle avoidance," *Proc. of the Int. Joint Conf. on Artificial Intelligence*, pp. 584-586, 1977.

[43] Mott-Smith, J. C. and Baer, T., "Area and volume coding of pictures," in *Picture Bandwidth Compression*, Eds. T. S. Huang and O. J. Tretiak, Gordon and Beach: New York, 1972.

[44] Noble, J. A., "Finding corners," *Image Vision Comput.*, vol. 6, pp. 121-128, 1988.

[45] Pavlidis, T., *Structural Pattern Recognition*, Springer, New York, pp. 161ff, 1977.

[46] Pei, Soo-Chang, Lai, Chin-Lun, and Shih, Frank Y., "A morphological approach to shortest path planning for rotating objects," *Pattern Recognition*, vol. 31, no. 8, pp. 1127-1138, 1998.

[47] Pennington, A., Bloor, M. S., and Balila, M., "Geometric modeling: A contribution toward intelligent robots," *13th International Symposium on Industrial Robots*, April 17-21, pp. 7.35-7.54, 1983.

[48] Pitas I. and Venetsanopoulos, A. N., "Nonlinear digital filters," Kluwer Academic Publishers, Boston, 1990.

[49] Pitas, I. and Venetsanopoulos, A. N., "Morphological shape decomposition," *IEEE Transactions on Pattern Analysis and Machine Intelligence*, vol. 12, pp. 38-45, 1990.

[50] Pratt, W. K. *Digital Image Processing*, Wiley, New York, pp. 530ff, 1978.

[51] Prewitt, J. M. S., "Object enhancement and extraction. In: Lipkin and Rosenfeld, Eds.," *Picture Processing and Psychopictorics.* Academic Press, New York, pp. 75-149, 1970.

[52] Ragothama, S. and Shapiro, V., "Boundary representation deformation in parametric solid modeling," *ACM Transactions on Graphics*, vol. 17, no. 4, pp. 259-286, 1998.

[53] Requicha, A. A. G., "Representations for rigid solids: theory, methods, and systems," *ACM Computing Surveys*, vol. 12, no. 4, pp. 437-464, December 1980.

[54] Requicha, A. A. G. and Voelcker, H. B., "Solid modeling: A historical summary and contemporary assessment," *IEEE Computer Graphics and Applications*, vol. 2, no. 2, pp. 9 –24, 1982.

[55] Requicha, A. A. G. and Voelcker, H. B., "Solid modeling: current status and research direction," *IEEE Computer Graphics and Applications*, vol. 3, pp. 25-37, Oct. 1983.

[56] Requicha, A. A. G., "Representation of tolerances in solid modeling: issues and alternative approaches," in *Solid Modeling by Computers*, Eds. J. W. Boyse and M. S. Pickett, Plenum, New York, pp. 3-12, 1984.

[57] Rosenfeld, A. and Johnston, E., "Angle detection on digital curves," *IEEE Trans. Computers*, C-22, pp. 875-878, 1973.

[58] Rosenfeld, A. and Kak, A. C., *Digital Picture Processing*, Academic Press, New York, pp. 371ff, 1976.

[59] Rosin, P. L., "Augmenting corner descriptors," *Graphical Models and Image Processing*, vol. 58, pp. 286-294, 1996.

[60] Rossignac, J., "CSG-Brep duality and compression," *Proc. ACM Symposium on Solid Modeling and Applications*, Saarbrucken, Germany, pp. 59-59, 2002.

[61] Rossignac, J. and Requicha, A. A. G., "Offsetting operations in solid modeling," Production Automation Project, University of Rochester, NY Tech. Memo, 53, June 1985.

[62] Russ, J. C., *The Image Processing Handbook*, CRC Press, 1992.

[63] Serra, J., *Image Analysis and Mathematical Morphology*, Academic Press, New York, 1982.

[64] Serra, J., "Introduction to mathematical morphology," *Comput. Vision, Graphics, Image Processing*, vol. 35, pp. 283-305, Sep. 1986.

[65] Shih, F. Y. and Cheng, Shouxian, "An adaptive morphological edge-linking algorithm," *IEEE Trans. Systems, Man, and Cybernetics*, in submission.

[66] Shih, F. Y., Gaddipati, V., and Blackmore, D., "Error analysis of surface fitting for swept volumes," *Proc. Japan-USA Symp. Flexible Automation*, Kobe, Japan, pp. 733-737, July 1994.

[67] Shih, F. Y. and Gaddipati, V., "General sweep mathematical morphology," *Pattern Recognition*, vol. 36, no. 7, pp. 1489-1500, July 2003.

[68] Shih, F. Y. and Mitchell, O. R., "Threshold decomposition of gray-scale morphology into binary morphology," *IEEE Trans. on Pattern Analysis and machine Intelligence*, vol. 11, no. 1, pp. 31-42, Jan. 1989.

[69] Shih, F. Y. and Mitchell, O. R., "Decomposition of gray-scale morphological structuring elements," *Pattern Recognition*, vol. 24, no. 3, pp. 195-203, 1991.

[70] Shih, F. Y. and Mitchell, O. R., "A mathematical morphology approach to euclidean distance transformation," *IEEE Trans. on Image Processing*, vol. 1, no. 2, pp. 197-204, April 1992.

[71] Shih, F. Y. and Pu, C.C., "Analysis of the properties of soft morphological filtering using threshold decomposition," *IEEE Trans. Signal Processing*, vol. 43, no. 2, pp. 539-544, 1995.

[72] Shih, F. Y.,"Object representation and recognition using mathematical morphology model," *Journal of Systems Integration*, vol. 1, pp. 235-256, 1991.

[73] Shih, F. Y. and Mitchell, O. R., "Threshold decomposition of gray-scale morphology into binary morphology," *IEEE Trans. on Pattern Analysis and machine Intelligence*, vol. 11, no. 1, pp. 31-42, Jan. 1989.

[74] Shiroma, Y., Kakazu, Y., and Okino, N., "A generalized sweeping method for CSG modeling," *Proc. of the First ACM Symposium on Solid Modeling Foundations and CAD/CAM Applications*, Austin, Texas, pp. 149-157, 1991.

[75] Shiroma, Y., Okino, N., and Kakazu, Y., "Research on 3-D geometric modeling by sweep primitives," *Proceedings of CAD 82*, Brighton, United Kingdom, pp. 671-680, 1982.

[76] Singh, A. and Shneier, M., "Gray level corner detection a generalization and a robust real time implementation," *Computer Vision Graphics and Image Processing*, vol. 51, pp. 54-69, 1990.

[77] Sinha D. and Dougherty, E.R., "Fuzzy mathematical morphology," *Journal of Visual Communication and Image Representation,* vol. 3, no. 3, pp. 286-302, September 1992.

[78] Smith, S. M. and Brady, J. M., "SUSAN – a new approach to low level image processing," *International Journal of Computer Vision*, vol. 23, no. 1, pp. 45-78, 1997.

[79] Song, X. and Neuvo, Y., "Robust edge detector based on morphological filters," *Pattern recognition Lett.*, vol. 14, pp. 889-894, 1993.

[80] Stevenson, R. L. and Arce, G. R., "Morphological filters: Statistics and further syntactic properties," *IEEE Trans. on Circuits and Systems*, vol. 34, no. 11, pp. 1292-1305, 1987.

[81] Tsai, Du-Ming, Hou, H. T., and Su, H. J., "Boundary-based corner detection using eigenvalues of covariance matrices," *Pattern Recognition Letters*, vol. 20, no. 1, pp. 31-40, 1999.

[82] Voelcker, H. B. and Hunt, W. A., "The role of solid modeling in machining process modeling and NC verification," SAE Tech. Paper #810195, 1981.

[83] Wang, W. P. and Wang, K. K., "Geometric modeling for swept volume of moving solids," *IEEE Computer Graphics and Applications*, vol. 6, no. 2, pp. 8-17, 1986.

[84] Wu, D. Q. and Brady, J. M., "A fast algorithm for morphological transformations," CV-3.1.6.

[85] Zadeh, L. A., "Fuzzy sets," *Inform. Control,* vol. 8, 1965.

[86] Zadeh, L. A., "Theory of fuzzy sets," in *Encyclopedia of Computer Science and Technology* (J. Belzer, A. Holzman, and A. Kent, eds.), Dekker, New York, 1977.

[87] Zheng, Zhiqiang, Wang, Han, and Teoh, Eam Khwang, "Analysis of gray level corner detection," *Pattern Recognition Letters*, vol. 20, pp. 149-162, 1999.

[88] Zuniga, O. A. and Haralick, R. M., "Corner detection using the facet model," *Proc. Conf. Computer Vision and Pattern Recognition,* pp. 30-37, 1983.